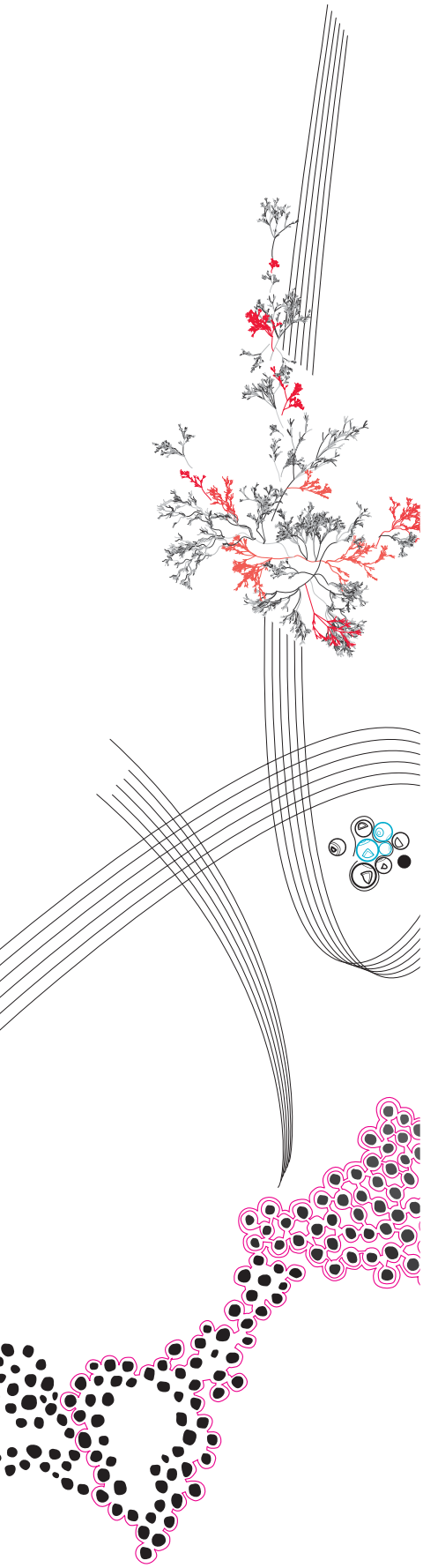

MSc Thesis Applied Physics

Solving the Hubble tension with a curvature dependent dark energy

Thijs van Rossum

Supervisor: Wim Beenakker, Radboud University Nijmegen
Second supervisor: Gerard Brocks

October, 2023

UNIVERSITY OF TWENTE.

ACKNOWLEDGEMENTS

I would like to thank everyone who has supported me and guided me through this master's thesis. First of all, I want to thank Wim Beenakker for his invaluable contribution and dedication to the project. This has made working on this thesis a very pleasant experience, which I won't take for granted. I also enjoy our weekly talks where I felt like we went through the scientific process in a proper way, which is a very valuable experience for me. Secondly, I would like to thank Bas van den Hoek, Tijmen Melssen and Jesse Cools who have been working on the same project along side me and were great sparring partners when needed. I finally want to thank all my friends and family for all their support during this demanding journey.

ABSTRACT

The Hubble parameter plays an important role to calculate astronomical distance and time intervals. Late and early universe measurements that apply the Λ-CDM model, show a mismatch between the Hubble parameter extrapolated to the present time. We propose an alternate model that replaces the cosmological constant Λ with a curvature dependent dark energy (CDDE) term, introducing a matter creation mechanism aimed to solve the Hubble tension. We were able to solve the Hubble tension by increasing the total matter content in the universe by 57% with light non-relativistic neutrinos with a rest mass energy of multiple meV. Our model is validated by comparing its predicted deceleration parameter against the Λ-CDM predicted version. Although our model was only constructed to solve the Hubble tension, it was also found to be compatible with the measured acceleration of the expansion of the universe. As an exploration of the matter creation mechanism we fitted our model to a two-component early universe consisting of radiation and baryonic matter exclusively. This increased the total matter content by a factor of 2.45, which is not enough to provide a consistent explanation for all the dark matter content in the universe. It is therefore not worthwhile to study the matter creation mechanism as a substitute for dark matter.

CONTENTS

1 INTRODUCTION

The Hubble parameter is an important parameter that is used to measure distances and time intervals in the cosmos. It describes the expansion rate of the universe and is commonly derived from the Λ-CDM standard model, which in turn is derived from the Einstein field equation with a cosmological constant Λ. It also includes Cold Dark Matter (CDM) in its model. This is motivated from several astrophysical observations such as gravitational lensing, galaxy rotation curves and the large scale structure. These observations cannot be explained with the amount of visible matter present. As an explanation to these phenomena, dark matter has been hypothesized as a type of matter that does not interact electromagnetically, making it very hard to detect. In the Λ-CDM model it is used to explain the discrepancy between the amount of matter measured in the late universe and the amount of baryonic matter derived from the epoch of Big Bang Nucleosynthesis (BBN), which is the epoch when the first nuclei were formed. See [1] for further details.

However, late and early universe observations have proposed seperate values for the Hubble constant, i.e. the present day Hubble parameter[2, 3, 4]. Different measurements on late universe observations are combined to get a Hubble constant of $H_0 = 73.3 \pm 0.8$ km/s/Mpc[2]. The Planck collaboration however did measurements on the Cosmic Microwave Background (CMB) and applied the Λ-CDM model to find a Hubble constant of $H_0 = 67.4 \pm 0.5$ km/s/Mpc[4]. This 'tension' potentially suggests that the Λ-CDM model is not yet complete and there is new physics left to explore[5].

In this study, we propose an alternative model to resolve the Hubble tension by replacing the cosmological constant Λ with a Curvature Dependent Dark Energy term (CDDE). This introduces an interactive term between dark energy and matter, which could increase the amount of matter in the universe when dark energy becomes an important energy density term in the universe. The underlying idea originates from Quantum Field Theory in curved spacetime. This theory predicts that particles can be created in the presence of a changing background metric.

As a follow-up, we will take this idea to the extreme and check if this mechanism can create enough matter to provide a consistent explanation for dark matter. This is done by fitting our model to an early-time two-component universe, which consists of baryonic matter and radiation exclusively.

In chapter 2, we start with a small history of the relevant history of the universe followed by the relevant theory behind the expansion of the universe. We will then discuss where we will deviate from the literature. In chapter 3, the methodology to solve the Hubble tension will be discussed. In addition, we will provide a method to fit our model to a universe that started out without dark matter. The results of these studies are discussed in chapter 4 followed by a conclusion and outlook in chapter 5.

2 THEORY

In this chapter the relevant context, followed by the theory behind this study will be discussed. The context and theory have been studied on the basis of [1]. We refer to this source for more details on the topics discussed in this chapter.

2.1 Small history of the universe

We will provide an overview of the history of the universe relevant for this study. Following the Big Bang and the epoch when protons and neutrons were formed the universe existed as a plasma comprising of baryonic matter (protons and neutrons), electrons, and radiation (photons and neutrinos). In addition the universe (most likely) contained a decoupled background of dark matter that mainly contributed gravitationally. The number of photons vastly outnumbers the number of baryons by a factor of $1.6 \cdot 10^9$ (see table 3.1)[6]. Therefore, photons played a leading role in the primordial plasma, which during early stages is completely radiation dominated. Figure 2.1 is an overview of the history of the universe, depicting the primordial plasma in more detail.

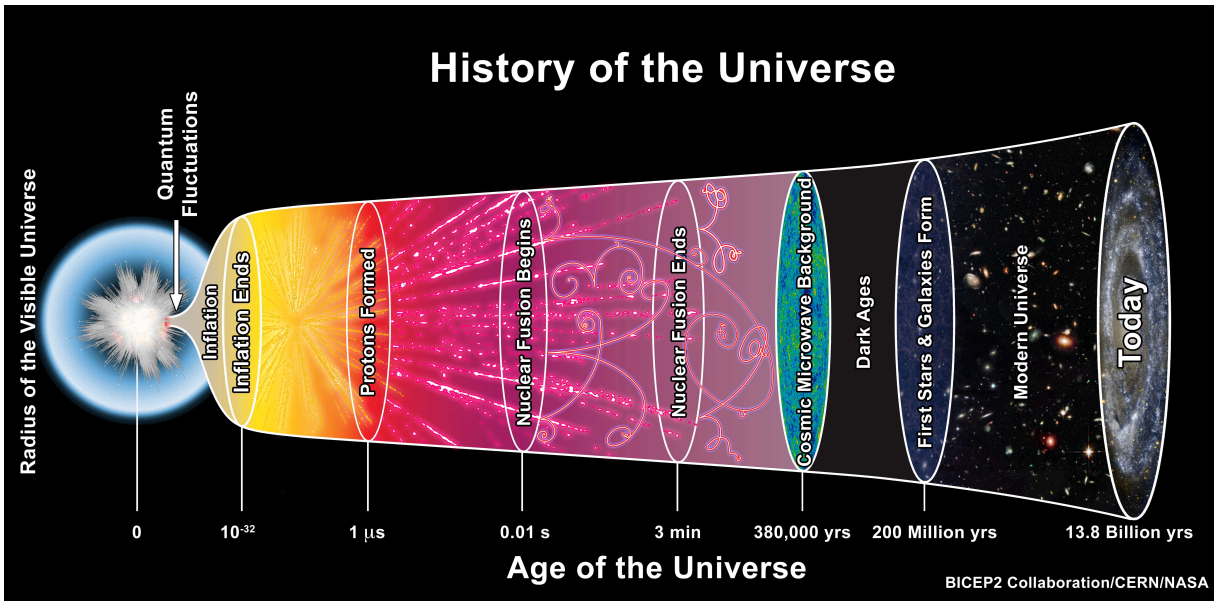

Figure 2.1: A visual aid of the history of the universe. Indicated are the most important events during the early universe. The time period relevant to this study is that after protons have been formed[7].

The approximate moment when the radiation-dominated universe ends is known as matter-radiation equality, when the energy density contributions of matter and radiation are equal. The moment of matter-radiation equality is model-dependent, but usually happens (well) before the primordial plasma disappears. While matter-radiation equality is an important ingredient for

describing structure formation, we will simply use it as a separator between the matter and radiation dominated universes. As we describe the primordial plasma, we will assume that electrons remained in thermal contact with the photons, and baryons maintained thermal contact with the electrons[8]. Because during this period all thermodynamic processes occurred much faster compared to the age of the universe, and given our previous assumption, we consider everything in the primordial plasma to be in thermal equilibrium. This means the thermodynamic processes are described through a Boltzmann distribution. Additionally, the average number of baryons and photons inside the plasma remains constant, while the radiation follows a Planck distribution and, in turn, describes the temperature of the plasma[9]. Because the universe is expanding, its components are diluted, lowering their matter/energy densities. As the photon energy density is related to temperature ($\rho_R \propto T^4$), the temperature of the universe also decreases. Consequently, thermodynamic processes within the plasma have only a brief window of opportunity to occur, as the universe's temperature transitions from 'too hot' to 'too cold. This means there is a chronological order to the thermodynamic processes that happen inside the primordial plasma, which will be described below.

An important epoch of thermodynamic processes happens at temperatures below $T \approx 3{\cdot}10^{10}\ K$ when the weak-interaction thermal equilibrium processes:

$$p + e^- \rightleftharpoons n + \nu_e \tag{2.1}$$

$$p + \bar{\nu}_e \rightleftharpoons n + e^+ \tag{2.2}$$

start to prefer protons over neutrons. At that time the positrons are still around as they can be formed by the electromagnetic process of electron-positron pair creation:

$$\gamma + \gamma \rightleftharpoons e^+ + e^- \tag{2.3}$$

The weak force interactions are mostly maintained by (anti-)neutrinos. However, as the universe expands the mean free path of the (anti-)neutrinos increases until it is larger than the Hubble length[10] at $T \approx 9{\cdot}10^9\ K$. The Hubble length is the distance which a hypothetical photon would have traveled in the expanding universe if it started moving from the Big Bang until a particular moment (in this case when $T \approx 9 \cdot 10^9\ K$). This causes the (anti-)neutrinos to decouple from the plasma, ending the epoch of weak force interactions 1s after the Big Bang. As a result, no more protons are turned into neutrons and the neutrons will decay into protons unless they are bonded to a stable atomic nucleus.

2.1.1 Big Bang Nucleosynthesis

From here the universe cools down to temperatures that allow fusion to occur. This epoch is called Big Bang Nucleosynthesis (BBN) and lasts for only a few minutes. The first fusion process happens at $T \approx 3 \cdot 10^9\ K$, when deuterium is fused from protons and neutrons:

$$n + p \rightleftharpoons D + \gamma \tag{2.4}$$

Deuterium is the first element to be formed because all other elements like helium-4 and beyond are fused from deuterium, although we will not consider elements beyond helium-4 in this study. There are various processes to fuse helium-4 from deuterium, by fusing intermediate products like helium-3 and tritium. These elements however fuse almost immediately into helium-4 so we will not look into the fusion process from deuterium to helium-4 in more detail. Even though the fusion temperature of helium-4 is higher than that of deuterium ($T \approx 2.6{\cdot}10^{11}\ K$), no helium-4 is formed because there is no deuterium to fuse with yet. As a result, the window of opportunity to fuse helium-4 is bottle-necked by the deuterium fusion process. In addition, during this process a small percentage of the neutrons decays back to protons, which slightly reduces the amount

of deuterium in the universe. The deuterium fusion process stops at $T \approx 7.6 \cdot 10^8 K$, which, in turn, stops all other fusion processes and 'freezes' the relative amounts of fused products compared to the number of unfused protons.

2.1.2 Photon decoupling

After the BBN epoch, the primordial plasma consists of ions in a sea of free electrons and photons with (potentially) a decoupled dark matter background that provides mainly a gravitational contribution. For example, the dark matter background interacts with the baryonic matter density fluctuations of the primordial plasma. This creates Baryonic Accoustic Oscillations (BAO) and plays a leading role in the structure formation after the primordial plasma has vanished[11, 12, 13]. The dominant interaction between all these components in the plasma is Thomson scattering between electrons and photons.

$$p + e^- \rightleftharpoons H + \gamma \tag{2.5}$$

As the universe is cooling down to a temperature of about $T \approx 3 \cdot 10^5\ K$, the photons reach the ionization energy of the ions, gradually allowing neutral atoms to be formed. This reduces the Thomson scattering rate since this requires free electrons that are not bound to atoms. Similarly to the neutrinos before the BBN epoch, this increases the mean free path of the photons until it is larger than the Hubble length and decouples the photons from the primordial plasma[10]. This happens at $T \approx 3 \cdot 10^3\ K$.

The photon radiation that we observe from the Cosmic Microwave Background (CMB) corresponds to the radiation the moment it was decoupled from the primordial plasma. This is still observed to follow a Planck (black-body) distribution at present time, proving the photons have been moving through the universe without interacting. Although the Planck distribution itself doesn't change, it redshifts over time, meaning we can calculate the radiation temperature after the photons have been decoupled. This is explained in more detail in table 3.1.

2.1.3 Universe after radiation dominance

After the photons have decoupled, the baryonic matter content in the universe 'freezes' because there is no more radiation that applies a pressure to the baryonic matter. This also means that the BAOs also are 'frozen' in place. These BAOs are observable in the cosmos[11, 12, 13, 14] (see figure 2.2). As the universe is expanding, the matter energy from the baryons (and dark matter) decreases at a slower rate than radiation, because the radiation wavelength increases along with the expansion of the universe, lowering its energy density even more. As a result, the matter energy density eventually exceeds the radiation energy density, creating a matter dominated universe.

This epoch comes to an end after enough time has passed for the matter energy density to be lower than the dark energy density. The exact moment when this happens is model dependent, but should happen when the radiation temperature reached $T \approx \mathcal{O}(10^1)\ K$. Because the dark energy density doesn't decrease in the same way as the matter and radiation energy densities during the expansion of the universe, the amount of energy in the universe effectively increases. This causes the universe to expand at an accelerating rate as observed in our present-day universe. The radiation temperature at present is $T = 2.73\ K$ (see table 3.1).

2.2 Expansion of the universe

In this thesis, we will apply the (+ - - -) signature convention for our metric. In addition, we will use natural units ($c = \hbar = \epsilon_0 = \mu_0 = k_B = 1$). By doing so, these constants become absorbed in the relevant quantities and fields. This allows us to express all units as powers of eV, which makes interpreting which particles can be created easier.

The theory of cosmology starts with general relativity, since gravity is the only predominant force at cosmological scales[15]. This is described by the Einstein field equations with a metric ($g_{\mu\nu}$) and dark energy term $\Lambda g_{\mu\nu}$ where $\Lambda > 0$:

$$G_{\mu\nu} + \Lambda g_{\mu\nu} = -8\pi G T_{\mu\nu} \tag{2.6}$$

Here G is the gravitational constant and the Einstein tensor ($G_{\mu\nu}$) is given by the traditional expression in the Einstein field equations in terms of the Ricci tensor ($R_{\mu\nu}$) and Ricci scalar (R):

$$G_{\mu\nu} = R_{\mu\nu} - \frac{1}{2} R g_{\mu\nu} \tag{2.7}$$

From observations of the large scale structure we know the large scale structure of the universe is homogeneous and isotropic. This is shown in figure 2.2, where at low distances there is a clear structure to the galaxy clusters in the universe, but as we go to higher distances this structure fades and the universe becomes homogeneous and isotropic.

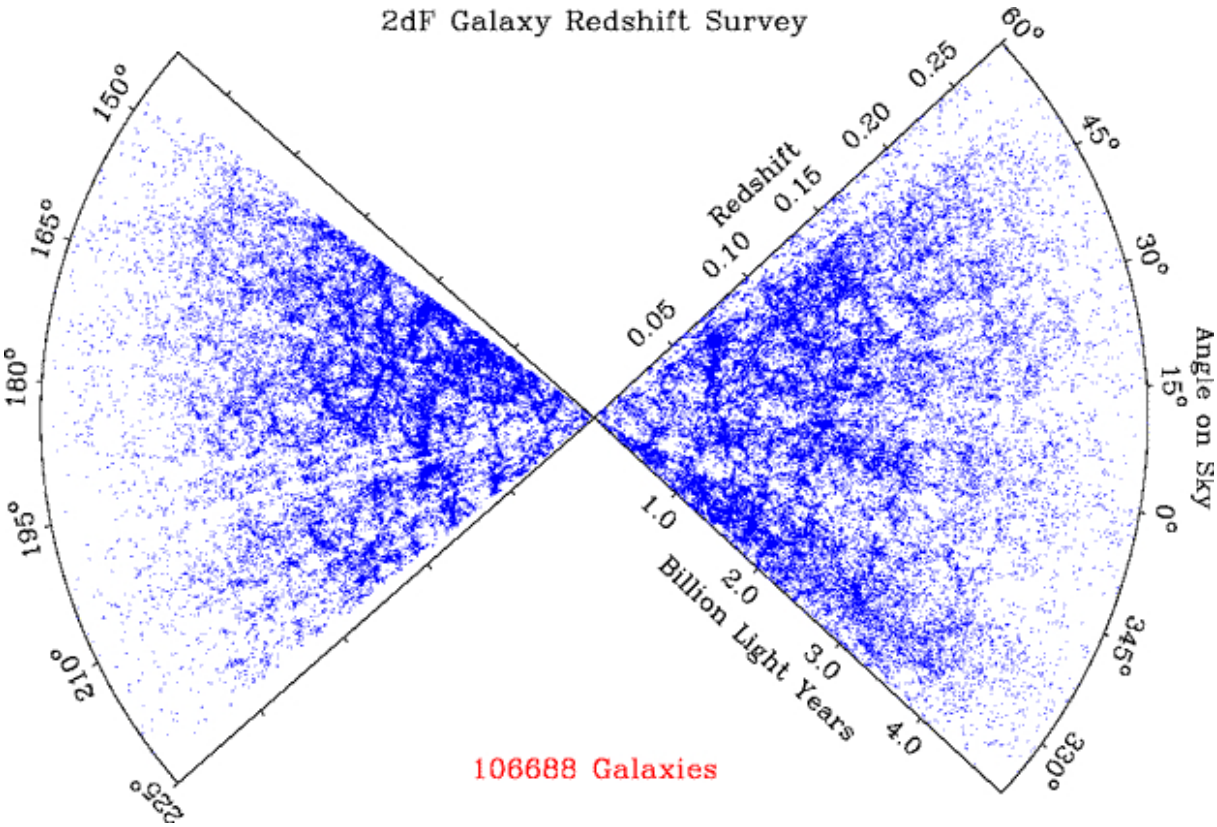

Figure 2.2: Observations of the cosmos at different angles and distances[14]. At low distances we clearly observe structure to the galaxy clusters, but as we observe the universe at larger distances this structure starts to disapear, rendering the large scale structure of the universe effectively homogeneous. This also happens at every angle, meaning the large scale structure of the universe is isotropic.

We therefore apply the perfect fluid approximation for our stress-energy tensor ($T_{\mu\nu}$):

$$T_{\mu\nu} = \textbf{\textit{diag}}(\rho, -pg_{ii}^{FRW}) \tag{2.8}$$

with i = 1,2,3 referring to the spacial components. Here ρ is the total energy density in the universe caused by non-relativistic matter (ρ_M) and radiation (ρ_R), consisting of super-relativistic matter and photons originating from the epoch of photon decoupling:

$$\rho = \rho_M + \rho_R \tag{2.9}$$

The $-pg_{ii}^{FRW}$ term is a pressure term which is caused by radiation with the relation:

$$p = \rho_R/3 \tag{2.10}$$

The perfect fluid approximation requires the metric of the universe $g_{\mu\nu}$ to be spherically symmetric. We therefore choose a metric with spherical symmetry and which is spatially scaled (with a scale factor $a(t)$) homogeneously and in an isotropic manner. Furthermore, the universe might have some intrinsic spatial curvature (κ), which we need to account for. Such a metric is called the Friedmann-Robertson-Walker (FRW) metric and is expressed in spatially spherical spacetime coordinates (t, r, θ, ϕ) as:

$$g_{\mu\nu}^{FRW} = \textbf{\textit{diag}}(1, -\frac{a^2(t)}{1-\kappa r^2}, -a^2(t)r^2, -a^2(t)r^2 \sin^2\theta) \tag{2.11}$$

By observing light emitted from distant galaxies, we can relate its redshift (z) to the scale factor:

$$a(z) = \frac{1}{1+z} \tag{2.12}$$

From this relation we define the scale factor at present time, denoted with a subscript 0 (t_0), to be 1 when no redshift is observed ($a(t_0) = a(z=0) \equiv 1$). Additionally, we will utilize the convention to use redshift as a surrogate for time. The motivation for this convention is apparent when calculating the comoving distance (D) of light traveling in an expanding universe from its emitted time (t_e) until the present (t_0):

$$D = \int_{t_e}^{t_0} \frac{dt}{a(t)} \tag{2.13}$$

Finding values for t_e, t_0 and $a(t)$ is barely measurable, since it requires knowing the absolute time of the universe. However, we can rewrite this equation in terms of z and define the Hubble parameter:

$$H = \frac{\dot{a}}{a} \tag{2.14}$$

where an overhead dot corresponds to differentiation with respect to time:

$$da = \dot{a}dt = -a^2 dz \tag{2.15}$$

$$\frac{dt}{a} = -\frac{adz}{\dot{a}} = -\frac{dz}{H(z)} \tag{2.16}$$

$$D = \int_0^{z_e} \frac{dz}{H(z)} \tag{2.17}$$

We can see that this integral is now expressed in terms of relative redshift, which can be measured directly. It also shows the importance of knowing the Hubble parameter in cosmology, for it is required in order to know any distance or quantity that evolves in time. In the upcoming sections we will explore two approaches to finding $H(z)$ from the Einstein field equations. While the Λ-CDM model assumes a cosmological constant as dark energy term, we will instead assume an alternative dynamical dark energy term depending on the Ricci scalar (R).

2.3 Hubble parameter according to Λ-CDM

The Λ-CDM model derives its version of the Hubble parameter by working out the Einstein field equations as explained in the previous section for a constant value of Λ:

$$R_{\mu\nu}(t) = \textit{diag}\left(3\frac{\ddot{a}(t)}{a(t)}, \left[\frac{\ddot{a}(t)}{a(t)} + 2H^2(t) + 2\frac{\kappa}{a^2(t)}\right] g_{ii}^{FRW}(t)\right) \tag{2.18}$$

$$R(t) = 6\left(\frac{\ddot{a}(t)}{a(t)} + H^2(t) + \frac{\kappa}{a^2(t)}\right) \tag{2.19}$$

We find there are only two unique equations ($\mu = \nu = 0$ and $\mu = \nu = i$).

Temporal part $G_{00} + \Lambda g_{00} = -8\pi G T_{00}$:

$$H^2(t) = \frac{8\pi G\rho(t) + \Lambda}{3} - \frac{\kappa}{a^2(t)} \tag{2.20}$$

Spatial part $G_{ii} + \Lambda g_{ii} = -8\pi G T_{ii}$:

$$\left[2\frac{\ddot{a}(t)}{a(t)} + H^2(t) + \frac{\kappa}{a^2(t)}\right] g_{ii}^{FRW} = -\left(8\pi G p(t) - \Lambda\right) g_{ii}^{FRW} \tag{2.21}$$

Using eqn. 2.20:

$$\frac{\ddot{a}(t)}{a(t)} - H^2(t) - \frac{\kappa}{a^2(t)} = -4\pi G[\rho(t) + p(t)] \tag{2.22}$$

Multiplying eqn 2.20 by $a^2(t)$ and taking the derivative with respect to time:

$$2\ddot{a}(t)\dot{a}(t) = \frac{8\pi G}{3}\left[2\dot{a}(t)a(t)\rho(t) + \dot{\rho}(t)a^2(t)\right] + 2\frac{\Lambda}{3}\dot{a}(t)a(t) \tag{2.23}$$

Rewriting eqn. 2.22 by inserting 2.20:

$$\frac{\ddot{a}(t)}{a(t)} = -\frac{4\pi G}{3}(\rho(t) + 3p(t)) + \frac{\Lambda}{3} \tag{2.24}$$

This expression shows that $\Lambda > 0$ could allow for an epoch with accelerated expansion. Combining the above eqn. with eqn. 2.23 results in the final differential eqn.

$$\dot{\rho}(t) = -3H(t)[\rho(t) + p(t)] \tag{2.25}$$

Eqns. 2.20 and 2.25 can be written in terms of z using eqn. 2.16 resulting in the following two unique equations:

$$H^2(z) = \frac{8\pi G\rho(z) + \Lambda}{3} - \kappa(1+z)^2 \tag{2.26}$$

$$\frac{d\rho(z)}{dz} = 3\frac{\rho(z) + p(z)}{1+z} \tag{2.27}$$

The above equations are however not solvable as we have three parameters ($H(z), \rho(z), p(z)$) but only two equations. To resolve this issue we will first rewrite $\rho(z)$ and $p(z)$ using eqns. 2.9 and 2.10:

$$H^2(z) = \frac{8\pi G(\rho_M(z) + \rho_R(z)) + \Lambda}{3} - \kappa(1+z)^2 \tag{2.28}$$

$$\frac{d\rho_M(z)}{dz} + \frac{d\rho_R(z)}{dz} = \frac{3\rho_M(z) + 4\rho_R(z)}{1+z} \tag{2.29}$$

Before solving the above equations we can rewrite eqn. 2.28 in an alternative form and define new dimensionless energy densities $\Omega_x(z) \equiv \frac{8\pi G}{3H^2(z)}\rho_x(z)$ to find an interesting result:

$$1 + \frac{\kappa(1+z)^2}{H^2(z)} = \Omega_M(z) + \Omega_R(z) + \Omega_\Lambda(z) \equiv \bar{\Omega}(z) \tag{2.30}$$

Note that Ω_Λ is traditionally defined as $\Omega_\Lambda(z) \equiv \frac{\Lambda}{3H^2(z)}$ so we will use this definition as well. The quantity $\bar{\Omega}$ is the dimensionless total energy density in the universe and depends on κ. This means that when the universe exhibits positive intrinsic spatial curvature (κ > 1) then $\bar{\Omega} > 1$, if the universe has no intrinsic spatial curvature (κ = 0) then $\bar{\Omega} = 1$ and in the case of negative intrinsic spatial curvature (κ < 1) then $\bar{\Omega} < 1$. Observing the large scale structure seems to support that the present universe is consistent with a spatially flat space-time, meaning $\kappa = 0$. It is therefore convenient to assume that $\kappa = 0$ for all times since it provides a simplification of our model and the Λ-CDM model with minimal error. Assuming $\kappa = 0$ also constrains Ω_x to be between 0 and 1, which helps with physical interpretations. We will therefore use Ω_x instead of ρ_x to describe energy densities. Eqn. 2.30 with $\kappa = 0$ is called the Benchmark model›:

$$\Omega_M(z) + \Omega_R(z) + \Omega_\Lambda(z) = 1 \tag{2.31}$$

Going back to eqns. 2.28 and 2.29, the Λ-CDM model makes the additional assumption that there is no interaction between matter and radiation. This is a safe assumption because the relevant time period of our study is after the epoch of photon decoupling. With this assumption, we can decouple eqn. 2.29 to obtain a third equation and giving the following expressions:

$$\rho_M(z) = \rho_{M,0}(1+z)^3 \tag{2.32}$$

$$\rho_R(z) = \rho_{R,0}(1+z)^4 \tag{2.33}$$

$$H^2(z) = \frac{8\pi G}{3}\rho_{M,0}(1+z)^3 + \frac{8\pi G}{3}\rho_{R,0}(1+z)^4 + \frac{\Lambda}{3} \tag{2.34}$$

We can rewrite eqn. 2.34 into the nicer form:

$$H^2(z) = H_0^2\left(\frac{8\pi G}{3H_0^2}\rho_{M,0}(1+z)^3 + \frac{8\pi G}{3H_0^2}\rho_{R,0}(1+z)^4 + \frac{\Lambda}{3H_0^2}\right) \tag{2.35}$$

$$\implies H(z) = H_0\sqrt{\Omega_{M,0}(1+z)^3 + \Omega_{R,0}(1+z)^4 + \Omega_{\Lambda,0}} \tag{2.36}$$

This is the final expression for $H(z)$ in the benchmark Λ-CDM model. Present day measurements of $\Omega_{M,0}^{\Lambda\text{-CDM}}$ and $\Omega_{R,0}$ show $\Omega_{R,0} = 7.74^{+0.178}_{-0.173}\cdot 10^{-5}$[16, 17] and $\Omega_{M,0}^{\Lambda\text{-CDM}} = 0.334 \pm 0.018$[18]. Here $\Omega_{R,0}$ is derived from late universe observations while $\Omega_{M,0}$ has been fit to match the data of [18]. See table 3.1 for more details. Note that the radiation energy density $\Omega_{R,0}$ includes ultra-relativistic and non-relativistic neutrinos. However, excluding non-relativistic neutrinos from the radiation energy density provides a negligible correction to $\Omega_{R,0}$ so it is not excluded in this study. Using eqn. 2.31, one can find the energy density due to dark energy $\Omega_{\Lambda,0} = 1 - \Omega_{R,0} - \Omega_{M,0}^{\Lambda\text{-CDM}} = 0.666^{+0.018}_{-0.018}$[16, 17, 18].

2.4 Alternative model

This study proposes an alternative dark energy model to describe the evolution of the universe. With this model, we assume dark energy interacts with matter by replacing Λ with a function of the Ricci scalar. This contains two of the ingredients listed in [5] that could solve the Hubble tension: a non-constant dark-energy density and matter that does not dilute $\propto a^{-3}$ (see below). We will sometimes call this the Curvature Dependent Dark Energy (CDDE) model. The

reason for having R as the argument of the function is that this maintains the homogeneity and isotropy of the universe. As a result, our dynamic dark energy term is dependent on the energy distribution of the universe:

$$\Lambda = 8\pi GC\sqrt{(R/6)} \tag{2.37}$$

The proportionality constant C is kept positive to have the same sign as Λ in order to allow for accelerated expansion. We apply the square root to the Ricci scalar as the lowest integer-dimensional dependence on R that is non-trivial and makes the expression dimensionally convenient. We can work out the Einstein field equations by substituting eqns. 2.37, 2.9 and 2.10 in the derivation of the Λ-CDM model from the previous section.

Temporal part $G_{00} + 8\pi GC\sqrt{(R/6)}g_{00}^{FRW} = -8\pi GT_{00}$:

$$H^2(t) + \frac{\kappa}{a^2(t)} = \frac{8\pi G}{3}\left[\rho_R(t) + \rho_M(t) + C\sqrt{\frac{\ddot{a}(t)}{a(t)} + H^2(t) + \frac{\kappa}{a^2(t)}}\right] \tag{2.38}$$

Spatial part $G_{ii} + 8\pi GC\sqrt{(R/6)}g_{ii}^{FRW} = -8\pi GT_{ii}$ combined with eqn. 2.38:

$$\frac{\ddot{a}(t)}{a(t)} - \left(H^2(t) + \frac{\kappa}{a^2(t)}\right) = -\frac{4\pi G}{3}\left[3\rho_M(t) + 4\rho_R(t)\right] \tag{2.39}$$

We define a new dark energy density $\beta \equiv \frac{16\pi GC^2}{3}$ which depends on our dynamical dark energy constant. With the help of eqn. 2.39 we can rewrite eqn. 2.38

$$\frac{\ddot{a}(t)}{a(t)} + \frac{4\pi G}{3}\left[\rho_M(t) + 2\rho_R(t)\right] = \frac{8\pi GC}{3}\sqrt{2\frac{\ddot{a}(t)}{a(t)} + \frac{4\pi G}{3}\left[3\rho_M(t) + 4\rho_R(t)\right]} \tag{2.40}$$

from which it follows that:

$$\left(\frac{\ddot{a}(t)}{a(t)}\right)^2 + \left(\frac{\ddot{a}(t)}{a(t)}\right)\frac{8\pi G}{3}(\rho_M(t) + 2\rho_R(t) - \beta) + \left(\frac{4\pi G}{3}\right)^2\left([\rho_M(t) + 2\rho_R(t)]^2 - \beta[3\rho_M(t) + 4\rho_R(t)]\right) = 0 \tag{2.41}$$

This equation is a second order polynomial which has two solutions. We choose the negative root solution because $C > 0$. It is interesting to note that in an empty universe ($\rho_M = \rho_R = 0$) with $C < 0$ solution results in a universe without cosmological constant. This means the universe could undergo a smooth phase transition from a universe with cosmological constant (De Sitter space) to one without cosmological constant as C goes from positive to negative:

$$\frac{\ddot{a}(t)}{a(t)} = -\frac{4\pi G}{3}\left[\rho_M(t) + 2\rho_R(t) - \beta - \beta\sqrt{1 + \frac{\rho_M(t)}{\beta}}\right] \tag{2.42}$$

Using eqn. 2.39:

$$H^2(t) + \frac{\kappa}{a^2(t)} = \frac{8\pi G}{3}\left[\rho_M(t) + \rho_R(t) + \frac{1}{2}\beta\left(1 + \sqrt{1 + \frac{\rho_M(t)}{\beta}}\right)\right] \tag{2.43}$$

We will get our next equation again by multiplying the above equation with $a^2(t)$ and taking the time derivative:

$$\dot{\rho}_M(t)\left(1 + \frac{1}{4\sqrt{1 + \frac{\rho_M(t)}{\beta}}}\right) + \dot{\rho}_R(t) = -H(t)(3\rho_M(t) + 4\rho_R(t)) \tag{2.44}$$

We encounter the same problem as in the Λ-CDM model. We have a set of equations (2.43, 2.44) with too many parameters ($H(t), \rho_M(t)$ and $\rho_R(t)$). In the next chapter we will derive a

substitution for the missing equation, based on the epoch of the universe where the error of introducing this equation is minimal. We will now show how a modified benchmark model is derived from eqn. 2.43 and use the same dimensionless energy densities as defined in the previous section ($\Omega_x(t) \equiv \frac{8\pi G}{3H^2(t)}\rho_x(t)$ as well as $\Omega_\beta(t) \equiv \frac{8\pi G}{3H^2(t)}\beta$):

$$1 + \frac{\kappa}{H^2(t)a^2(t)} = \frac{8\pi G}{3H^2(t)}\left[\rho_M(t) + \rho_R(t) + \frac{1}{2}\beta\left(1 + \sqrt{1 + \frac{\rho_M(t)}{\beta}}\right)\right]$$

$$= \Omega_M(t) + \Omega_R(t) + \frac{1}{2}\Omega_\beta(t)\left(1 + \sqrt{1 + \frac{\Omega_M(t)}{\Omega_\beta(t)}}\right) \equiv \bar{\Omega}(t) \tag{2.45}$$

Just like with Λ-CDM if $\bar{\Omega} > 1$ this demands $\kappa > 1$ and $\bar{\Omega} < 1$ means $\kappa < 1$. Assuming $\kappa = 0$ therefore requires $\bar{\Omega} = 1$ and constrains $\Omega_M, \Omega_R, \Omega_\beta \in [0, 1]$. Substituting $\kappa = 0$ in 2.45 results in the benchmark model for our dynamical dark energy model:

$$\Omega_M(t) + \Omega_R(t) + \frac{1}{2}\Omega_\beta(t)\left(1 + \sqrt{1 + \frac{\Omega_M(t)}{\Omega_\beta(t)}}\right) = 1 \tag{2.46}$$

To summarize, we will write our final equations in terms of z instead of t:

$$\Omega_M(z) + \Omega_R(z) + \frac{1}{2}\Omega_\beta(z)\left(1 + \sqrt{1 + \frac{\Omega_M(z)}{\Omega_\beta(z)}}\right) = 1 \tag{2.47}$$

$$\frac{d\rho_M(z)}{dz}\left(1 + \frac{1}{4\sqrt{1 + \frac{\rho_M(z)}{\beta}}}\right) + \frac{d\rho_R(z)}{dz} = \frac{3\rho_M(z) + 4\rho_R(z)}{1 + z} \tag{2.48}$$

We see that these equations are similar to the equations from the Λ-CDM model, but have an additional interactive term between ρ_M and β. This term will describe how matter is created from dark energy and its effect will be important once $\rho_M \leq \mathcal{O}(\beta)$. To solve the Hubble tension, we will start with data from the late universe and numerically evolve $\rho_M(z), \rho_R(z)$ and $H(z)$ towards the past. We will fit β such that H at the epoch of photon decoupling (H_*) will match the Λ-CDM based Hubble parameter derived from measurements of the early universe ($H_*^{\Lambda\text{-CDM}}$)[4].

This fit condition was chosen because at the end of photon decoupling, dark energy has a negligible contribution in our model as well as in the Λ-CDM framework. This means there is no noticeable difference between the two models, given that we assume the same amount of dark matter in our model as in the Λ-CDM model. There is however a difference when translating CMB data to our model due to matter creation effects that should be accounted for. These matter creation effects could also play a role in the initial density fluctuations in the CMB. This is presently being explored in a different study by another researcher working on the same project.

3 METHODOLOGY

In this chapter, we will discuss our methodology to solve the Hubble tension as well as the method for our follow-up study. The context behind these methods is based on [1]. We refer to this source for more details.

3.1 Identifying Λ-CDM-Independent quantities

Our proposed model departs from the assumptions of the Λ-CDM framework which means that parameter values derived from Λ-CDM cannot be directly utilized. This poses a significant challenge as Λ-CDM stands as the standard cosmological model and forms the foundation for astronomical observations. The following table gives an overview of commonly used parameters and their model dependencies.

Quantity	Value	Λ-CDM Independent?	Source
H_0^{early}	67.4 ± 0.5 km/s/Mpc	No	Measured at CMB and extrapolated to z = 0 with equation 3.1[4]
H_0^{late}	73.3 ± 0.8 km/s/Mpc	Yes	Low z observations[2, 5]
Temperature $T(z)$	$T(z) = T_0(1+z)$ $T_0 = 2.72548K \pm 0.57mK$	Yes	Calculated from the blackbody radiation observed from the CMB[16][1].
$\Omega_{M,0}^{\Lambda\text{-CDM}}$	0.334 ± 0.018	No	Fitted to the data of supernova surveys[18]. The implied Hubble parameter corresponds to H_0^{late}
$\Omega_{R,0}$	$7.74^{+0.178}_{-0.173} \cdot 10^{-5}$	Yes	Derived from $T(z)$ and H_0^{late}. This derivation includes the contribution from neutrinos and photons[2, 16, 17, 5]
Helium to Baryon ratio Y	0.2479 ± 0.0029	Yes	The authors of [19] reviewed multiple studies on Y and concluded the study of [20] produced the best value
Baryon-Photon ratio η	$(6.14 \pm 0.25) \cdot 10^{-10}$	Slight dependence[2]	Abundance observations that are matched to abundance models (see figure 3.3)[6]

Table 3.1: Table with used quantities in this study and their Λ-CDM dependencies.

3.2 Solving the Hubble tension

The basic requirement of solving the Hubble tension is to find a function $H(z)$ that successfully intersects the measured data points in both the early ($H_*^{\Lambda\text{-CDM}}$) and late (H_0^{late}) universe. We will assume H_* has been acquired by means of eqn. 2.36:

$$H_*^{\Lambda\text{-CDM}} = H_0^{early}\sqrt{\Omega_{M,0}^{\Lambda\text{-CDM}}(1+z_*)^3 + \Omega_{R,0}^{\text{early}}(1+z_*)^4 + \Omega_{\Lambda,0}^{\text{early}}} \tag{3.1}$$

Here $\Omega_{R,0}^{\text{early}} = 9.16^{+0.314}_{-0.299}\cdot 10^{-5}$ is derived in the same way as described in table 3.1, but the implied Hubble parameter now corresponds to H_0^{early} instead of H_0^{late}. This is not applied to $\Omega_{M,0}^{\Lambda\text{-CDM}}$ because this has been fitted directly to the data in [18]. These parameters are derived in the same way as in [4] so to follow their procedure, we will treat $\Omega_{M,0}^{\Lambda\text{-CDM}}$ and $\Omega_{R,0}^{\text{early}}$ in the same way. Consequently, the value of $\Omega_{\Lambda,0}^{\text{early}} = 1 - \Omega_{M,0}^{\Lambda\text{-CDM}} - \Omega_{R,0}^{\text{early}} = 0.67^{+0.018}_{-0.018}$. The exact value of z_* will be derived in a later section of this chapter. Our method to finding $H(z)$ will be done by numerically evolving our model (eqns. 2.47 and 2.48). These equations are however not optimized for numerical computation and will therefore be modified. We will rewrite our current parameters ($H(z)$, $\rho_M(z)$ and $\rho_R(z)$) into more suitable quantities and rewrite our model's equations accordingly.

3.2.1 Transforming to numerically suitable equations

We will transform our parameters to the following quantities:

- $\rho_M(z) \to \Omega_M(u)$
- $\rho_R(z) \to \Omega_R(u)$
- $z \to u = \ln(1+z)$
- $H(z) \to \ln[H(u)/H_0^{\text{late}}] := \ln(H(u))$

For the transformation of $H(z)$, we divide by H_0^{late} to gain a dimensionless argument in the logarithm. However, to maintain readability of the equations, we will omit explicitly writing down this division. This does not alter the equations themselves. The latter two transformations lead to the following chain rule identities which will be used to derive our numerically suitable equations:

$$\frac{d}{dz} = \frac{du}{dz}\frac{d}{du} = \frac{1}{1+z}\frac{d}{du} \tag{3.2}$$

$$\frac{1}{H(z)}\frac{dH(z)}{dz} = \frac{d\ln(H(z))}{dz} \tag{3.3}$$

[1] The radiation wavelength, after decoupling from the primeval plasma, is assumed to increase by a factor of $a = 1/(1+z)$ as it travels through space in an expanding universe. The observed temperature is thus: $T \propto \lambda^{-1} \propto 1+z \Longrightarrow T \propto (1+z)$. This is still true when the radiation is coupled to matter but the reason is now because the plasma is in thermal equilibrium, which means the photons follow a planck distribution [8]

[2] The abundance models are based on a set of closely timed thermodynamic processes. In particular, the amount of neutrons that are formed before BBN and the number of neutrons that have decayed back to protons during the BBN are all time dependent processes and therefore calculated by means of the Hubble parameter. However, the Hubble parameter during this time is described by a one component radiation dominated universe, which is in accordance with our model.

Transforming eqn. 2.47 will be done by taking the derivative with respect to z:

$$\frac{d}{dz}\left[\Omega_M+\Omega_R+\frac{1}{2}\Omega_\beta\left(1+\sqrt{1+\frac{\rho_M}{\beta}}\right)\right]=0$$
$$=\left(\Omega_M+\Omega_R+\frac{1}{2}\Omega_\beta\left(1+\sqrt{1+\frac{\rho_M}{\beta}}\right)\right)H^2\frac{d}{dz}H^{-2}+\frac{8\pi G}{3H^2}\left[\frac{d\rho_M}{dz}\left(1+\frac{1}{4\sqrt{1+\frac{\rho_M}{\beta}}}\right)+\frac{d\rho_R}{dz}\right] \tag{3.4}$$

Next inserting eqns. 2.47 and 2.48 yields:

$$H^2\frac{d}{dz}H^{-2}+\frac{8\pi G}{3H^2}\left(\frac{3\rho_M+4\rho_R}{1+z}\right)=0$$
$$\implies -2\frac{d\ln H}{dz}=-\frac{3\Omega_M+4\Omega_R}{1+z}$$
$$\implies \frac{d\ln H}{du}=\frac{3\Omega_M+4\Omega_R}{2} \tag{3.5}$$

Next we transform eqn. 2.48 by substituting the transformation equation from $\rho_{M,R}$ to $\Omega_{M,R}$:

$$\frac{d\Omega_{M,R}}{dz} = \frac{8\pi G}{3H^2}\frac{d\rho_{M,R}}{dz}+\frac{8\pi G}{3H^2}\rho_{M,R}\left(H^2\frac{dH^{-2}}{dz}\right) = \frac{8\pi G}{3H^2}\frac{d\rho_{M,R}}{dz}-2\Omega_{M,R}\frac{d\ln H}{dz}$$
$$\implies \frac{8\pi G}{3H^2}\frac{d\rho_{M,R}}{dz}=\Omega_{M,R}\left(\frac{3\Omega_M+4\Omega_R}{1+z}\right)+\frac{d\Omega_{M,R}}{dz} \tag{3.6}$$

Substituting this equation in eqn. 2.48:

$$\frac{8\pi G}{3H^2}\left[\frac{d\rho_M}{dz}\left(1+\frac{1}{4\sqrt{1+\frac{\rho_M}{\beta}}}\right)+\frac{d\rho_R}{dz}\right]=\frac{8\pi G}{3H^2}\left[\frac{3\rho_M+4\rho_R}{1+z}\right] \tag{3.7}$$

yields:

$$\left[\frac{d\Omega_M}{dz}+\Omega_M\left(\frac{3\Omega_M+4\Omega_R}{1+z}\right)\right]\left(1+\frac{1}{4\sqrt{1+\frac{\Omega_M}{\Omega_\beta}}}\right)+\left[\frac{d\Omega_R}{dz}+\Omega_R\left(\frac{3\Omega_M+4\Omega_R}{1+z}\right)\right]=\left(\frac{3\Omega_M+4\Omega_R}{1+z}\right)$$

$$\implies \frac{d\Omega_M}{dz}\left(1+\frac{1}{4\sqrt{1+\frac{\Omega_M}{\Omega_\beta}}}\right)+\frac{d\Omega_R}{dz}=\left(\frac{3\Omega_M+4\Omega_R}{1+z}\right)\left[1-\Omega_M\left(1+\frac{1}{4\sqrt{1+\frac{\Omega_M}{\Omega_\beta}}}\right)-\Omega_R\right]$$

$$\implies \frac{d\Omega_M}{du}\left(1+\frac{1}{4\sqrt{1+\frac{\Omega_M}{\Omega_\beta}}}\right)+\frac{d\Omega_R}{du}=(3\Omega_M+4\Omega_R)\left[1-\Omega_M\left(1+\frac{1}{4\sqrt{1+\frac{\Omega_M}{\Omega_\beta}}}\right)-\Omega_R\right]$$

Our final expressions that are fit for numerical computation are:

$$\frac{d\ln H}{du}=\frac{3\Omega_M+4\Omega_R}{2} \tag{3.8}$$

$$\frac{d\Omega_M}{du}\left(1+\frac{1}{4\sqrt{1+\frac{\Omega_M}{\Omega_\beta}}}\right)+\frac{d\Omega_R}{du}=(3\Omega_M+4\Omega_R)\left[1-\Omega_M\left(1+\frac{1}{4\sqrt{1+\frac{\Omega_M}{\Omega_\beta}}}\right)-\Omega_R\right] \tag{3.9}$$

3.2.2 Fitting parameter and initial conditions

To solve the Hubble tension, we will fit our dark energy term β, such that our resulting Hubble parameter fits the requirements stated in the beginning of this chapter. Considering that our energy densities are expressed as Ω_x instead of ρ_x, it is logical to employ $\Omega_{\beta,0}$ as a fitting parameter instead of β. This substitution poses no issue as $\Omega_{\beta,0} = \frac{8\pi G}{3(H_0^{late})^2}\beta$, with the proportionality constant being independent of the Λ-CDM model (See table 3.1). As for the numerical method, it is required to specify an initial condition (In $H_0^{late}, \Omega_{M,0}$, and $\Omega_{R,0}$) from which the evolution into the past can be computed. We will express $\Omega_{M,0}$ in terms of the fitting parameter ($\Omega_{\beta,0}$) with our benchmark model (see eqn. 2.47). This is necessary because $\Omega_{M,0}^{\Lambda\text{-CDM}}$ is a Λ-CDM dependent parameter and thus cannot be utilized. This also makes $\Omega_{M,0}$ a good candidate to be a free parameter, which is needed for the implementation of a fitting parameter.

3.2.3 Introducing a third equation for the epoch after photon decoupling

As explained in the previous chapter, a third equation is required to solve the set of differential equations in our model. Consequently, we will assume the radiation (ρ_R) in the universe is decoupled at photon decoupling and simply propagates independently from matter (ρ_M) and dark energy (β). This is motivated from the fact that the observed radiation power spectrum has a black body characteristic[4, 9, 16]. Any interactions between radiation and matter or dark energy after photon decoupling would disrupt the black body pattern. As this is not the case, we can conclude that radiation follows the Stephan-Boltzmann relation (see table 3.1):

$$\rho_R \propto (1+z)^4 \Longrightarrow \rho_R(z) = \rho_{R,0}(1+z)^4 \tag{3.10}$$

From this we can use eqn. 3.6 to find the third equation for our model.

$$\begin{aligned}
\frac{8\pi G}{3H^2}\left(\frac{4\rho_R(z)}{1+z}\right) &= \Omega_R\left(\frac{3\Omega_M + 4\Omega_R}{1+z}\right) + \frac{d\Omega_R}{dz} \\
\Longrightarrow \frac{d\Omega_R}{dz} &= \frac{4\Omega_R}{1+z} - \Omega_R\left(\frac{3\Omega_M + 4\Omega_R}{1+z}\right) \\
\Longrightarrow \frac{d\Omega_R}{du} &= 4\Omega_R - \Omega_R\left(3\Omega_M + 4\Omega_R\right)
\end{aligned} \tag{3.11}$$

3.2.4 Determining z_*

Our assumption for a third equation is defined to be valid after the epoch of photon decoupling when radiation is decoupled from matter. We will therefore derive the exact decoupling moment to provide a clear endpoint for our numerical simulation. The derivation starts by considering the universe when matter and radiation are still coupled. The universe was then simply an expanding sphere of plasma consisting of photons in a sea of free electrons and baryonic matter. In addition, the universe contained a decoupled background of neutrinos and dark matter that only interact very weakly and therefore formally are not part of the plasma. However, they do play a role gravitationally through the scale factor evolution (Hubble parameter). Note that at a later stage in this thesis we will omit the dark matter component from the background in our follow-up study. During this epoch the number of scattering events between matter and radiation are dominated by Thomson scattering between photons and electrons. The scattering rate of this process (Γ) is defined as:

$$\Gamma(z) = n_e(z)\sigma \tag{3.12}$$

Here n_e is the number density of electrons available for scattering and σ is the Thomson scattering cross-section ($\sigma = 6.65 \cdot 10^{-29}\ m^2$). This cross-section is multiplied by the relative electron

flux experienced by each photon, which equals n_e for a relative velocity of $v_{rel} = c = 1$ between electrons and photons. We will define the time of decoupling (z_*) when the expansion rate of the universe (the Hubble parameter) is equal to the Thomson scattering rate:

$$\frac{\Gamma(z_*)}{H(z_*)} \equiv 1 \tag{3.13}$$

To determine $n_e(z)$, we will assume a neutrally charged plasma consisting exclusively of unbound electrons, hydrogen, helium-4 and their respective ions. The total mass energy density contributions of electrons are omitted from the matter energy density of the plasma, as their masses are negligible compared to the masses of hydrogen and helium-4, with only the baryonic component ρ_b remaining. From observations of the large scale structure, the mass density percentage of helium-4 is approximately 24%[19, 20]. This percentage will be denoted with the parameter Y:

$$Y = \rho(\text{He-4})/\rho_b \tag{3.14}$$

We will also write down the charge of any particle/element in the number density, such that n_{He0} represents the number density of neutrally charged helium and n_{He1} represents He^+ etc. The exception to this notation applies to electrons, because they are the only particles present with a negative charge. From these observations and assumptions we can write down the following equations:

$$\rho_b(z) = m_{\text{H0}}[n_{\text{H0}}(z) + n_{\text{H1}}(z)] + m_{\text{He0}}[n_{\text{He0}}(z) + n_{\text{He1}}(z) + n_{\text{He2}}(z)] \tag{3.15}$$

$$Y\rho_b(z) = m_{\text{He0}}[n_{\text{He0}}(z) + n_{\text{He1}}(z) + n_{\text{He2}}(z)] \tag{3.16}$$

$$(1-Y)\rho_b(z) = m_{\text{H0}}[n_{\text{H0}}(z) + n_{\text{H1}}(z)] \tag{3.17}$$

$$n_e(z) = n_{\text{H1}}(z) + n_{\text{He1}}(z) + 2n_{\text{He2}}(z) \tag{3.18}$$

Because the masses of hydrogen and helium are about the same as their respective ions, we have only used the neutrally charged masses for simplicity. Next, we will assume the universe has had enough time for any adaptive change to reach thermal equilibrium[9]. Consequently, the particle density of any particle/element n_{xi} with charge i and mass m_{xi} in the plasma follows a Boltzmann distribution:

$$n_{xi}(z) = g_{xi}\left(\frac{m_{xi}T(z)}{2\pi}\right)^{3/2}\exp\left(-\frac{m_{xi}}{T(z)}\right) \tag{3.19}$$

Here g_{xi} is the statistical spin weight of the particle/element (for example, electrons with spin 1/2 have $g_e = 2$). From this equation we can derive the Saha equation, which expresses the ion number densities in terms of their ionization energy to go from a neutral/ionized element to the next ionized element. For example to go from H to H^+ or from He^+ to He^{2+}[21].

$$\frac{n_{x(i+1)}(z)n_e(z)}{n_{xi}(z)} = \frac{g_e g_{x(i+1)}}{g_{xi}}\left(\frac{m_{x(i+1)}m_e T(z)}{m_{xi}2\pi}\right)^{3/2}\exp\left[-\frac{m_{x(i+1)}+m_e-m_{xi}}{T(z)}\right]$$

$$\implies \frac{n_{x(i+1)}(z)n_e(z)}{n_{xi}(z)} = \frac{2g_{x(i+1)}}{g_{xi}}\left(\frac{m_e T(z)}{2\pi}\right)^{3/2}\exp\left(-\frac{Q_{x(i+1)}}{T(z)}\right) \equiv f_{x(i+1)}(z)$$

$$\implies n_{x(i+1)}(z) = \frac{n_{xi}(z)}{n_e(z)}f_{x(i+1)}(z) \tag{3.20}$$

In the tables below an overview is given of the spin statistical weight and ionization energy for each ion/element.

Element/Ion	Nucleus spin	Electron spin	g
H0	1/2	1/2	4
H1	1/2	0 (no electron)	2
He0	0	0	1
He1	0	1/2	2
He2	0	0 (no electron)	1

Table 3.2: Spins and spin statistical weights of hydrogen, helium and their respective ions.

Ionization of hydrogen	$Q_{\mathsf{H1}} = 13.54eV$	$2g_{\mathsf{H1}}/g_{\mathsf{H0}} = 1$
First ionization of helium	$Q_{\mathsf{He1}} = 24.48eV$	$2g_{\mathsf{He1}}/g_{\mathsf{He0}} = 4$
Second ionization of helium	$Q_{\mathsf{He2}} = 51.17eV$	$2g_{\mathsf{He2}}/g_{\mathsf{He1}} = 1$

Table 3.3: Ionization energies and ratio of spin statistical weights of hydrogen and helium ions.

Using eqn. 3.20 we can rewrite all ion number densities in eqns. 3.16 and 3.17 to their respective neutrally charged version:

$$Y\rho_b = m_{\mathsf{He0}}\left(1 + \frac{f_{\mathsf{He1}}}{n_e} + \frac{f_{\mathsf{He1}}f_{\mathsf{He2}}}{n_e^2}\right) n_{\mathsf{He0}}$$

$$\implies Y\rho_b = \frac{m_{\mathsf{He0}}}{n_e^2}\left(n_e^2 + f_{\mathsf{He1}}n_e + f_{\mathsf{He1}}f_{\mathsf{He2}}\right) n_{\mathsf{He0}}$$

Simplifying the expression by substituting the second order polynomial:

$$P_2 = m_{\mathsf{He0}}\left(n_e^2 + f_{\mathsf{He1}}n_e + f_{\mathsf{He1}}f_{\mathsf{He2}}\right)$$

$$\implies Y\rho_b = \frac{P_2}{n_e^2} n_{\mathsf{He0}}$$

$$\implies n_{\mathsf{He0}} = \frac{n_e^2}{P_2} Y\rho_b \tag{3.21}$$

Now applying the same method to eqn. 3.17:

$$(1-Y)\rho_b = m_{\mathsf{H0}}\left(1 + \frac{f_{\mathsf{H1}}}{n_e}\right) n_{\mathsf{H0}}$$

$$\implies (1-Y)\rho_b = \frac{m_{\mathsf{H0}}}{n_e}\left(n_e + f_{\mathsf{H1}}\right) n_{\mathsf{H0}} \tag{3.22}$$

Simplifying the above expression with $P_1 = m_{\mathsf{H0}}\left(n_e + f_{\mathsf{H1}}\right)$:

$$(1-Y)\rho_b = \frac{P_1}{n_e} n_{\mathsf{H0}}$$

$$\implies n_{\mathsf{H0}} = \frac{n_e}{P_1}(1-Y)\rho_b \tag{3.23}$$

Now rewriting eqn. 3.18:

$$n_e = \frac{f_{\mathsf{H1}}}{n_e} n_{\mathsf{H0}} + \left(\frac{f_{\mathsf{He1}}}{n_e} + 2\frac{f_{\mathsf{He1}}f_{\mathsf{He2}}}{n_e^2}\right) n_{\mathsf{He0}}$$

$$\implies n_e = \frac{f_{\mathsf{H1}}}{n_e} n_{\mathsf{H0}} + \frac{\left(f_{\mathsf{He1}}n_e + 2f_{\mathsf{He1}}f_{\mathsf{He2}}\right)}{n_e^2} n_{\mathsf{He0}}$$

$$\implies n_e = \frac{f_{\mathrm{H1}}}{P_1}(1-Y)\rho_b + \frac{(f_{\mathrm{He1}} n_e + 2 f_{\mathrm{He1}} f_{\mathrm{He2}})}{P_2} Y \rho_b$$
$$\implies P_1 P_2 n_e = P_2 f_{\mathrm{H1}}(1-Y)\rho_b + (f_{\mathrm{He1}} n_e + 2 f_{\mathrm{He1}} f_{\mathrm{He2}})\, P_1 Y \rho_b \tag{3.24}$$

Expanding P_1 and P_2 in terms of n_e gives us a fourth order polynomial:

$$\begin{aligned}
& m_{\mathrm{H0}} m_{\mathrm{He0}} n_e^4 + \\
& (f_{\mathrm{H1}} m_{\mathrm{H0}} m_{\mathrm{He0}} + f_{\mathrm{He1}} m_{\mathrm{H0}} m_{\mathrm{He0}})\, n_e^3 + \\
& (f_{\mathrm{H1}} f_{\mathrm{He1}} m_{\mathrm{H0}} m_{\mathrm{He0}} + f_{\mathrm{He1}} f_{\mathrm{He2}} m_{\mathrm{H0}} m_{\mathrm{He0}} - Y f_{\mathrm{He1}} m_{\mathrm{H0}} \rho_b + (Y-1) f_{\mathrm{H1}} m_{\mathrm{He0}} \rho_b)\, n_e^2 + \\
& (f_{\mathrm{H1}} f_{\mathrm{He1}} f_{\mathrm{He2}} m_{\mathrm{H0}} m_{\mathrm{He0}} - Y f_{\mathrm{H1}} f_{\mathrm{He1}} m_{\mathrm{H0}} \rho_b - 2Y f_{\mathrm{He1}} f_{\mathrm{He2}} m_{\mathrm{H0}} \rho_b + (Y-1) f_{\mathrm{H1}} f_{\mathrm{He1}} m_{\mathrm{He0}} \rho_b)\, n_e + \\
& -2Y f_{\mathrm{H1}} f_{\mathrm{He1}} f_{\mathrm{He2}} m_{\mathrm{H0}} \rho_b + (Y-1) f_{\mathrm{H1}} f_{\mathrm{He1}} f_{\mathrm{He2}} m_{\mathrm{He0}} \rho_b = 0
\end{aligned}$$

Finding the right root branch is a matter of calculating the coefficients and computing the roots during the numerical evolution. We then take the root branch that is positive and real. Luckily for this application, there is only one positive real root branch so there is no problem in choosing one. With this expression we find z_* by computing the ratio $\Gamma(z)/H(z)$ during the simulation and finding the z value where this ratio equals 1.

3.2.5 Fitting method

As mentioned in section 2.2.2, we will fit $\Omega_{\beta,0}$ to solve the Hubble tension. This will be done by means of a binary searching algorithm. During the numerical evolution, we calculate the ratio of $\Gamma(z)/H(z)$ and halt the backward evolution when this ratio reaches 1. We label the redshift value at which the evolution stops as z_* and use equation 3.1 to compute $H_*^{\Lambda\text{-CDM}}$. Comparing this value to $H(z_*)$ obtained from the numerical evolution reveals how $\Omega_{\beta,0}$ must be adjusted for $H(z_*)$ to approach $H_*^{\Lambda\text{-CDM}}$. This process is repeated until $H(z_*) \approx H_*^{\Lambda\text{-CDM}}$ within a specified tolerance. This method simultaneously fits values for z_* and $\Omega_{\beta,0}$ such that the Hubble tension is solved. Figures 3.1 and 3.2 provide a graphical illustration of the fitting method.

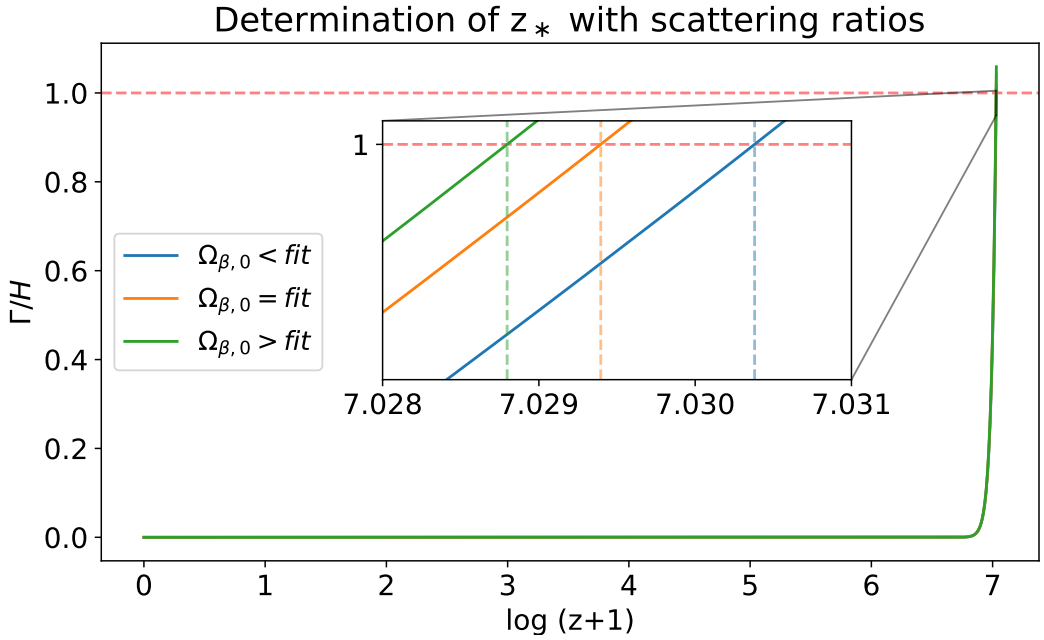

Figure 3.1: Ratio between the Thomson scattering rate and expansion rate of the universe. The vertical dashed lines show the value of z_*. The $\Omega_{\beta,0}$ values have been chosen to show the effect of changing $\Omega_{\beta,0}$ above and below the fitted value and have been chosen arbitrarily. In the next figure, we will use this redshift value to determine $H_*^{\Lambda\text{-CDM}}$.

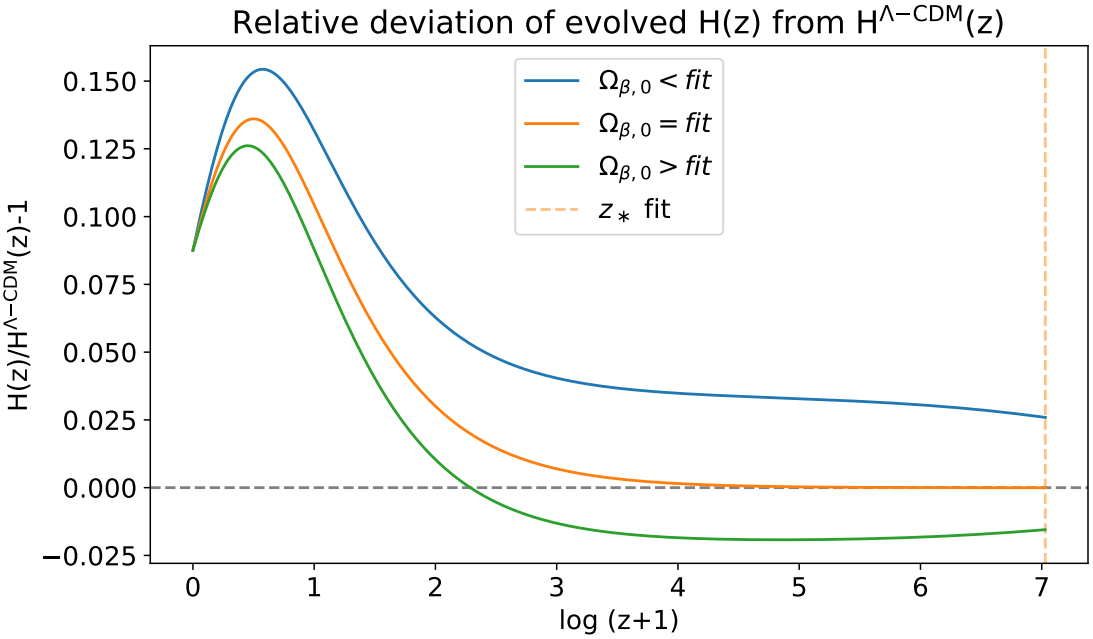

Figure 3.2: The relative deviation of the evolved $H(z)$ from $H^{\Lambda\text{-CDM}}(z)$. The impact of the Hubble tension is evident in the graph, as the initial value of the graph at $\log(z+1) = 0$ is equal to $H_0^{\text{late}}/H_0^{\text{early}} - 1$. The fitting condition of our model requires that the deviation should vanish at z_*, which was found from figure 3.1, indicated by the vertical dashed line.

The plot in figure 3.2 can be subdivided into three different epochs. The first epoch is when $H(z) \approx H^{\Lambda\text{-CDM}}(z)$ at high z. In the early universe, the deviation from Λ-CDM should be low because the dark energy contribution is almost negligible in the early universe. After this epoch the dark energy contribution starts increasing, which increases the acceleration rate of the universe and in turn increases $H(z)$ relative to $H^{\Lambda\text{-CDM}}(z)$. This causes dark energy to create matter at an increasing rate, which decreases the dark energy dominance somewhat, resulting in a decreasing effect of $H(z)$ relative to $H^{\Lambda\text{-CDM}}(z)$ at low z.

The binary search algorithm to solve the Hubble tension is an iterative method which oscillates around the correct value of $\Omega_{\beta,0}$. We can see this is a delicate process from figures 3.1 and 3.2. Different values of $\Omega_{\beta,0}$ result in a very small shift in the value of z_* (figure 3.1), but this small shift results in a substantial difference in $H(z_*)$ (figure 3.2).

3.3 Model validity

We will test the validity of our model against the deceleration parameter $q_0 = -\frac{\ddot{a}}{aH^2}\big|_{t=t_0}$. This is used for late universe observations by means of a Taylor expansion, which exhibits low error and Λ-CDM independent input[15]. Additionally, we expect our deviation from the Λ-CDM model to be largest at low z:

$$H^{\text{late}}(z) \approx H_0^{\text{late}} + \frac{dH(z)}{dz}\Big|_{z=0} z + ... \tag{3.25}$$

$$\implies H^{\text{late}}(z) \approx H_0^{\text{late}} \left(1 + \left[\frac{a^2}{\dot{a}}\left(\frac{\dot{a}}{a} - \frac{\ddot{a}}{\dot{a}}\right)\right]\Big|_{t=t_0} z\right)$$

$$= H^{\text{late}}(z) \approx H_0^{\text{late}} \left(1 + (1+q_0)z\right) \tag{3.26}$$

The Taylor expansion relies on knowing two parameter values: H_0^{late} and the deceleration parameter q_0. Given that our model already shares the same H_0^{late} value by definition, we will confront the q_0 values produced by our model with those reported in the literature. This validation method has been chosen because the datasets that are necessary to fit our CDDE model to the Λ-CDM model are not available to the people involved in this project.

3.4 Integrated effect

We will showcase the integrated effect of our model by looking at the amount of matter that is created or annihilated during the numerical evolution. Specifically, we will examine the ratio between the amount of matter present at two points in time: at z_* and at the present time, $z = 0$. This ratio is equivalent to the matter density multiplied by its associated volume, which scales as $V(z) \propto (1+z)^{-3}$. This mass-creation factor is given by:

$$f_M = \frac{\rho_M(0)(1+0)^{-3}}{\rho_M(z_*)(1+z_*)^{-3}} = \frac{\rho_M(0)(1+z_*)^3}{\rho_M(z_*)} = \frac{\Omega_{M,0}H_0^2(1+z_*)^3}{\Omega_M(z_*)H_*^2} \tag{3.27}$$

This expression is applicable to our CDDE model as well as to the Λ-CDM model. Note that in the Λ-CDM model, H_0 = H_0^{early} and $f_M = 1$ because the total number of non-relativistic particles doesn't change in the Λ-CDM model. This is handled differently in our CDDE model because $H_0 = H_0^{\text{late}}$ and $f_M > 1$ due to the matter-creation mechanism.

In our follow-up study we will use f_M to check if the amount of created matter could consistently explain the amount of predicted dark matter. According to existing literature, this should be about a factor of 5 or 6 [1]. It is important to note that experimental data always comes with an associated margin of error. Thus, we will analyze the overlap between the error margins of our model and the experimentally measured version. This analysis will be conducted using the min-max method[22], where we repeat the fit for every combination of high and low values from our experimental data

3.5 Follow-up study

With this follow-up study, we will (almost) completely depart from the Λ-CDM model by fitting our model as described in section 3.2.5, but instead replacing $H_*^{\Lambda\text{-CDM}}$ (see eqn. 3.1) with H_*, which is described by a two-component universe consisting of radiation $\Omega_{R,0}$ and baryons $\Omega_{b,0}$ (dark energy is technically also present along with very few non-relativistic neutrinos but this provides a negligible contribution in this case):

$$H_* = H_0^{\text{late}}\sqrt{\Omega_{b,0}(1+z_*)^3 + \Omega_{R,0}(1+z_*)^4} \tag{3.28}$$

The baryonic matter density $\Omega_{b,0}$ is derived from the constant baryon-photon number density ratio $\eta = n_b/n_\gamma$. This is derived from a (mostly) Λ-CDM independent calculation of the fusion rates during the epoch of Big Bang Nucleosynthesis (BBN). Calculations on the BBN provide predictions about the abundance ratios of deuterium, helium-4 and higher order elements against hydrogen, which can be measured from spectral line intensities from galaxies.[6]. These abundance ratios are all dependent on η, but the deuterium/hydrogen ratio (D/H) puts the largest constraint on η[6]. This is evident from figure 3.3, where the WMAP group plotted the abundance ratios as a function of η[6]. We will however not use the deuterium/hydrogen ratio in our model as it represents a negligible contribution to the total mass density.

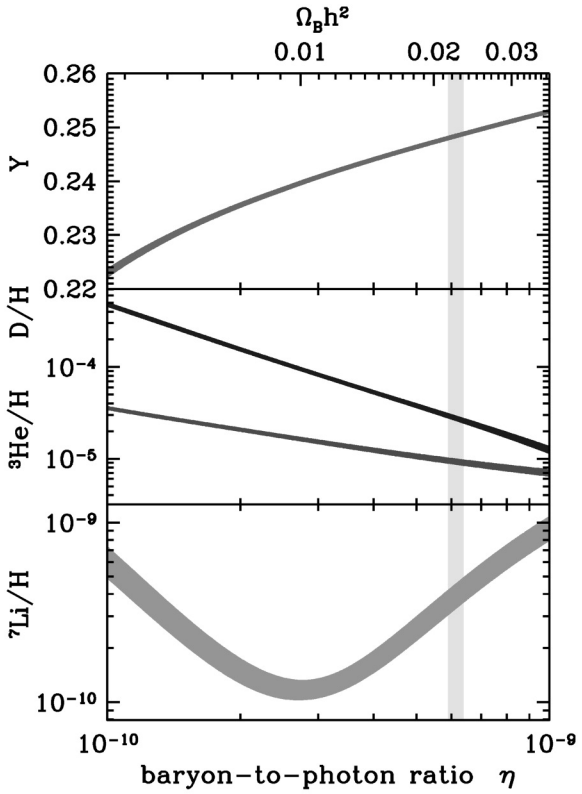

Figure 3.3: WMAP model of element abundances against η. By measuring the abundance ratios the baryon-to-photon ratio can be derived. It was found that $\eta = (6.14 \pm 0.25) \cdot 10^{-10}$. The D/H dependence on η in this graph shows how this measurement has a large impact on η. Note that the measured Ω_b is multiplied by $h^2 = (H_0/100[\text{km/s/Mpc}])^2$. This is done in order to remove the issues related to the Hubble tension from the Ω_b measurement.[6]

With a given value for η, we can determine the number density of baryons by means of the photon number density (n_γ). This is well-established because the photon energy density follows a Planck distribution, which, in turn, defines the photon number density as follows:

$$n_\gamma(z) = 0.243T^3(z) = 0.243[T_0(1+z)]^3 \tag{3.29}$$

$$n_b(z) = \eta n_\gamma(z) \tag{3.30}$$

Using the above equations, we can find an expression for $\Omega_{b,0}$:

$$\Omega_{b,0} = \frac{8\pi G}{3(H_0^{\text{late}})^2}\rho_{b,0} \tag{3.31}$$

$$\rho_{b,0} = m_b n_{b,0} = m_b \eta n_\gamma(0) \tag{3.32}$$

Here m_b is the average baryon mass, derived from eqns 3.16 and 3.17:

$$\rho_b = \frac{m_{\text{H0}}(n_{\text{H0}} + n_{\text{H1}})}{(1-Y)} = \frac{m_{\text{He0}}(n_{\text{He0}} + n_{\text{He1}} + n_{\text{He2}})}{Y} \tag{3.33}$$

$$\begin{aligned} n_b &= n_{\text{H0}} + n_{\text{H1}} + 4[n_{\text{He0}} + n_{\text{He1}} + n_{\text{He2}}] \\ &= \left[1 + 4\frac{m_{\text{H0}}Y}{(1-Y)m_{\text{He0}}}\right](n_{\text{H0}} + n_{\text{H1}}) \\ &= \left[1 + 4\frac{m_{\text{H0}}Y}{(1-Y)m_{\text{He0}}}\right]\frac{\rho_b(1-Y)}{m_{\text{H0}}} \end{aligned} \tag{3.34}$$

$$= \left[\frac{(1-Y)}{m_{\mathsf{H0}}} + 4\frac{Y}{m_{\mathsf{He0}}}\right]\rho_b$$

$$\implies \rho_b(z_*) = \left[\frac{m_{\mathsf{He0}}m_{\mathsf{H0}}}{m_{\mathsf{He0}}(1-Y)+4m_{\mathsf{H0}}Y}\right] n_b(z_*) \equiv m_b\eta n_\gamma(z_*) \tag{3.35}$$

$$m_b = \frac{m_{\mathsf{He0}}m_{\mathsf{H0}}}{m_{\mathsf{He0}}(1-Y)+4m_{\mathsf{H0}}Y} \tag{3.36}$$

Reinserting the above equation into eqns. 3.31 and 3.32:

$$\Omega_{b,0} = \frac{8\pi G}{3(H_0^{\mathsf{late}})^2}\left[\frac{m_{\mathsf{He0}}m_{\mathsf{H0}}}{m_{\mathsf{He0}}(1-Y)+4m_{\mathsf{H0}}Y}\right]\eta\ 0.243\ T_0^3 \tag{3.37}$$

we find $\Omega_{b,0} = 0.0443^{+0.00269}_{-0.00258}$ using table 3.1.

4 RESULTS AND DISCUSSION

4.1 Overview of the fit and evolution

After performing the fit procedure as described in the previous chapter, we find $z_* = 1128.35^{+2.37}_{-2.35}$ and $\Omega_{\beta,0} = 0.465^{+0.033}_{-0.034}$. With this value we can evaluate the initial value $\Omega_{M,0}$ using eqn. 2.46. This results in $\Omega_{M,0} = 0.443^{+0.030}_{-0.029}$. Because of the extra interactive term in eqn. 2.46, our value of $\Omega_{M,0}$ is a bit higher than $\Omega^{\Lambda\text{-CDM}}_{M,0}$. With all initial conditions established, we can now carry out the numerical evolution and present a rundown of the universe by plotting the evolved energy densities.

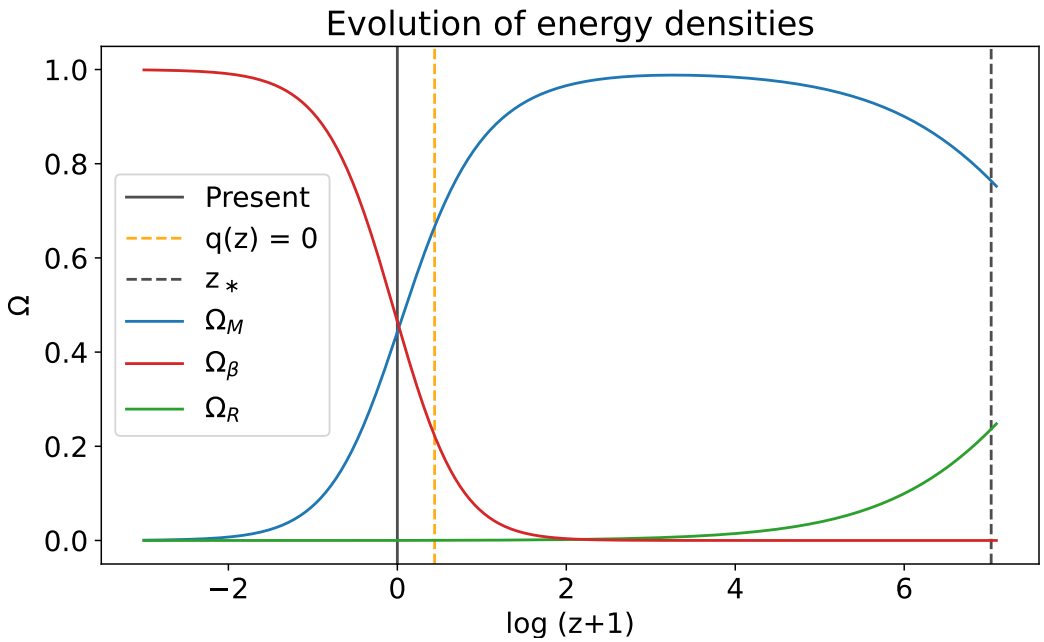

Figure 4.1: This graph provides a visual representation of the various epochs of the universe, as described in chapter 1, leading up to photon decoupling. By computing log(z+1) directly, we can evolve energy densities into the future, from which we see that our model predicts that eventually dark energy will be the only dominant constituent of the universe. Furthermore, the benchmark model is depicted within the graph, with segments in each epoch of the universe indicating energy densities summing up to 1. Figure 4.2 provides an illustrative depiction of this summation.

4.1.1 Deviation from Λ-CDM

In this section, we show how our model deviates from Λ-CDM. A preview of this model difference is already given in figure 3.2, showcasing the evolution of our fitted Hubble parameter compared to the Hubble parameter from the Λ-CDM model. Additionally, we will showcase the

most significant divergence from the Λ-CDM benchmark model, offering a region where our model can be validated.

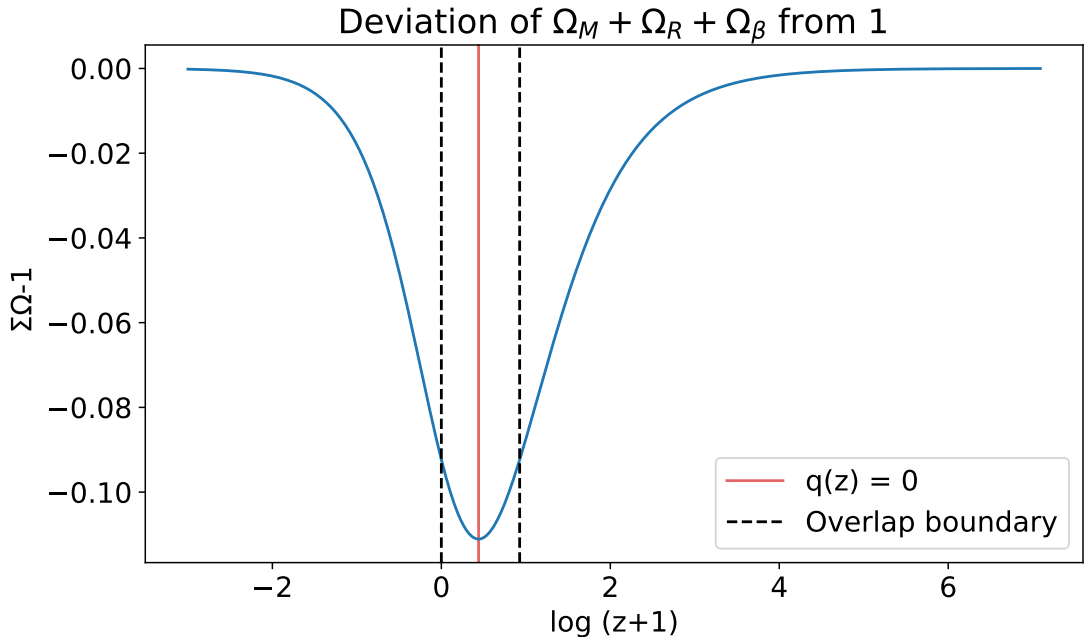

Figure 4.2: The difference between the sum of all the evolved energy densities in our model and 1, with the dark energy contribution replaced by the Ω_β term from the asymptotically constant dark energy density β. This shows how far our model deviates from the Λ-CDM benchmark model (eqn. 2.31). As a sidenote, our model predicts the deviation from the Λ-CDM model to be the largest when $q(z) = 0$. We wish to validate our model in the region where our difference from Λ-CDM is the largest, while the experimental data is the most accurate. According to this graph, if we are looking for a validation region where the difference with the Λ-CDM model exceeds the difference at present time, then the validation of our model should be carried out within the interval $z \in [0, 1.527]$ as is depicted with the black dashed lines.

Figure 4.2 shows how our dynamical dark energy term differs from the traditional cosmology with a constant dark energy term. The $z = 0$ point on the plot indicates that we are not yet in the regime with a cosmological constant and won't be in this regime for the foreseeable future. By treating our dynamical dark energy term Ω_β in the same manner as the cosmological constant in the Λ-CDM model Ω_Λ, our benchmark model (eqn. 2.47) can be rewritten as:

$$\Omega_M + \Omega_R + \Omega_\beta = 1 + \frac{1}{2}\Omega_\beta \left(1 - \sqrt{1 + \frac{\Omega_M}{\Omega_\beta}}\right) \tag{4.1}$$

We see that the right hand side of this equation is always ≤ 1 because $1 \leq \sqrt{1 + \frac{\Omega_M}{\Omega_\beta}}$. This negative term on the right hand side represents the excess energy stored in the ground state of the universe beyond a cosmological constant. This explains why our Hubble parameter indeed eventually becomes larger than the Hubble parameter in the Λ-CDM model, depending on Ω_β and redshift z (see figure 3.2). This aspect has allowed us to solve the Hubble tension within our model. As can be seen in figure 4.2, this effect is largest in the late universe, thereby allowing us to solve the Hubble tension by fitting $\Omega_{\beta,0}$. We see the additional term on the right hand side of eqn. 4.1 effectively vanishes in the very late universe when $\Omega_\beta \gg \Omega_M$ and thus $1 - \sqrt{1 + \frac{\Omega_M}{\Omega_\beta}} \approx$

0. This happens as well in the early universe where $\Omega_\beta \ll \Omega_M$, since $\Omega_\beta \left(1 - \sqrt{1 + \frac{\Omega_M}{\Omega_\beta}}\right) \approx -\sqrt{\Omega_M \Omega_\beta} \approx 0$ compared to Ω_M.

4.1.2 Model validation: accelerated expansion

The differential effect of our model will be validated in the redshift interval derived from figure 4.2, where we will check whether our model is able to both solve the Hubble tension and make a correct prediction for the accelerated expansion of the universe. In the previous section we provided a validation region according to our CDDE model. However, we also want to determine an experimentally required best overlap region based on the data sample from the literature used in this study. In particular, we will find a best overlap region from the measurement of $\Omega_{M,0}^{\Lambda\text{-CDM}}$ from the Pantheon+Sh0ES dataset[18].

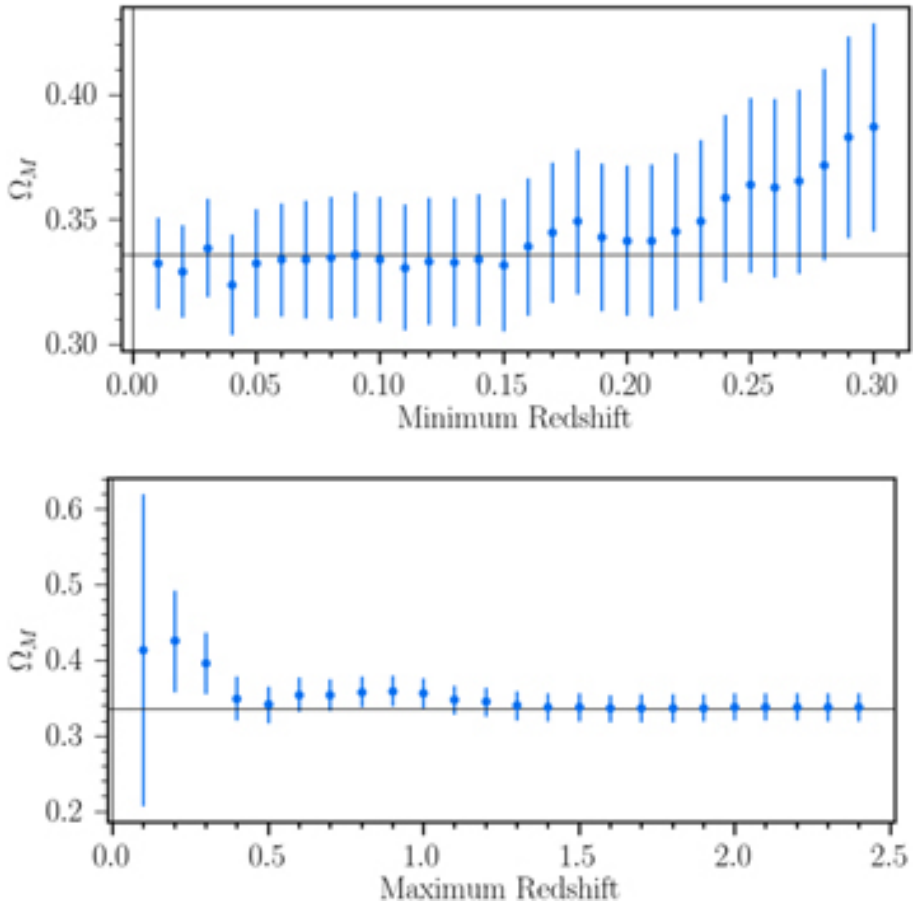

Figure 4.3: Measurement of $\Omega_{M,0}^{\Lambda\text{-CDM}}$ from the Pantheon+SH0ES dataset upon varying the maximum and minimum redshift of the measurement sample [18]. We see that Ω_M converges as the sample includes redshifts higher than $z \approx 1$. This means that values beyond $z \approx 1$ don't provide a meaningful contribution to the value of $\Omega_{M,0}^{\Lambda\text{-CDM}}$. Similarly, we see that $\Omega_{M,0}^{\Lambda\text{-CDM}}$ converges at redshift values lower than $z \approx 0.15$. This means our experimentally required best overlap region should ideally be between $z \approx 0.15$ and $z \approx 1$, which falls inside the validation region defined in fig. 4.2

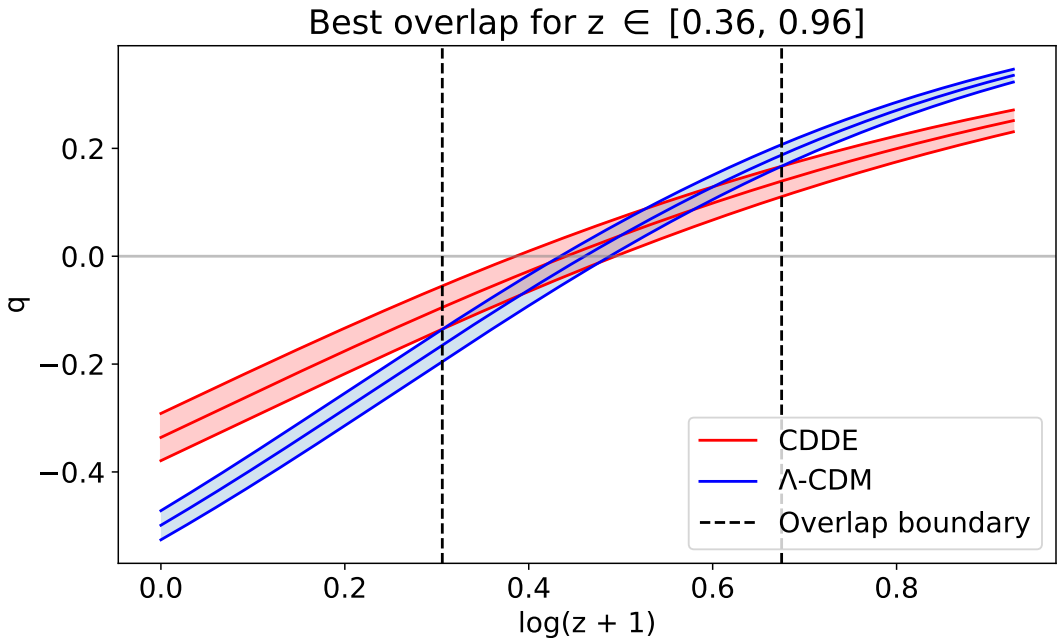

Figure 4.4: The deceleration parameter for low redshift for the Λ-CDM model (blue) and our alternative model (red) in the validation region according to fig. 4.2. The width of the CDDE band is larger due to the larger error of $\Omega_{M,0}$ in the CDDE model compared to $\Omega_{M,0}^{\Lambda\text{-CDM}}$.

We see in figure 4.4 that the best overlap region for $q(z)$ between both models is located where the deviation from Λ-CDM is inherently the largest (see figure 4.2), with an almost perfect overlap between the two models at $q = 0$. The overlap region between the two models largely covers the entire experimentally required best overlap region from figure 4.3.

We can conclude from figure 4.4 that our CDDE model's predicted acceleration shows significant overlap with the Λ-CDM model within the established validation region and the experimentally required region of best overlap. This is not a trivial result because the CDDE model is only constructed to solve the Hubble tension. The presence of such overlap in the deceleration parameter occurs naturally within the model. It implies that the CDDE model can solve the Hubble tension and at the same time still be consistent with the observed acceleration of the late universe.

4.1.3 Integrated effect: matter creation until present time

To observe the matter creation/annihilation mechanism of our model, we imagine $\rho_M(z)$ can be expressed as $\rho_M(z) = \rho_{M,0}(1+z)^{B(z)}$, where $B(z)$ is the power law. If $B > 3$, we speak of matter annihilation and if $B < 3$, matter is created. If $B = 3$ no matter creation or annihilation takes place, as this describes a fixed amount of matter in a volume that expands proportional to $a^3 = (1+z)^{-3}$. As can be seen from the figure below, we observe matter creation at redshifts below $z \approx 9$. This is in agreement with the mass-creation factor, which yields $f_M = 1.57$ for this study.

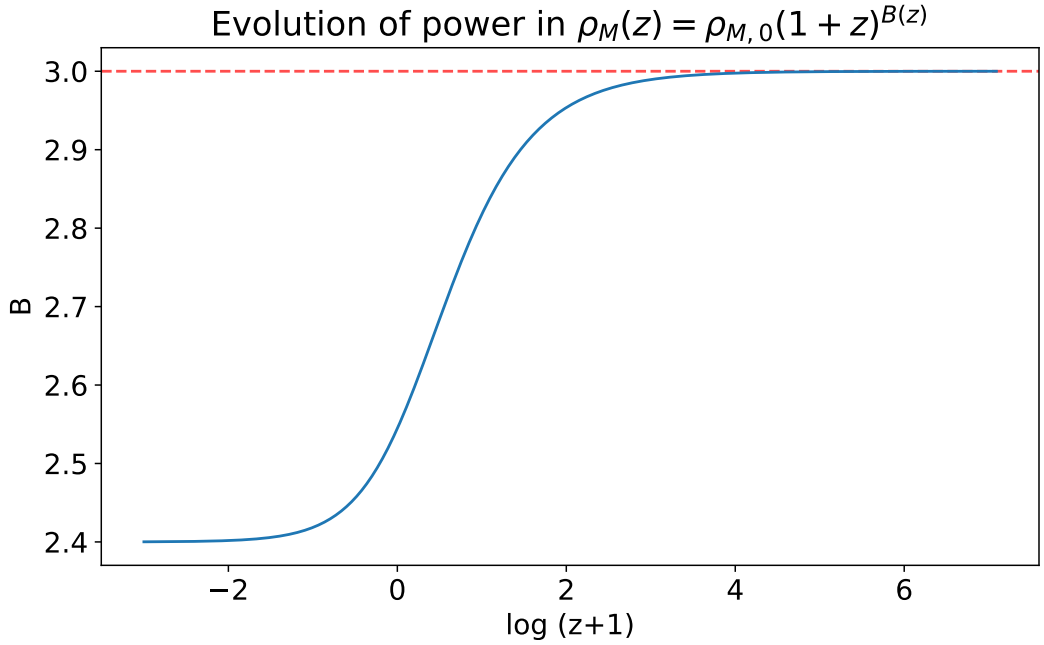

Figure 4.5: The evolution of the power law with which $\rho_M(z)$ reduces. In the early universe, we see $B = 3$, corresponding to no matter creation or annihilation. This is expected because our model behaves the same as the Λ-CDM model during this period (see figure 4.2). We see that that the matter creation starts to have a significant contribution at around $z \approx 9$, resulting in an ultimate future power law of $B = 2.4$.

4.1.4 Discussion

Our first study has successfully solved the Hubble tension. As a side effect, our model also predicts that 57% more matter has been created over time on top of the amount present in the Λ-CDM framework. The types of particles that can be created are loosely related to the energy scale of our dark energy density ρ_{DE} which has the unit $[\text{eV}^4]$:

$$\Omega_M + \Omega_R + \frac{1}{2}\Omega_\beta \left(1 + \sqrt{1 + \frac{\Omega_M}{\Omega_\beta}}\right) = \Omega_M + \Omega_R + \Omega_{\text{DE}}$$

$$\implies \rho_{\text{DE}}(z) = \frac{1}{2}\Omega_\beta(z) \left(1 + \sqrt{1 + \frac{\Omega_M(z)}{\Omega_\beta(z)}}\right) \frac{3H(z)^2}{8\pi G} \tag{4.2}$$

In figure 4.6, the dark energy scale $\rho_{\text{DE}}^{1/4}$ is plotted against the temperature of the CMB in order to get an impression of the energy scale of the particles that could be created.

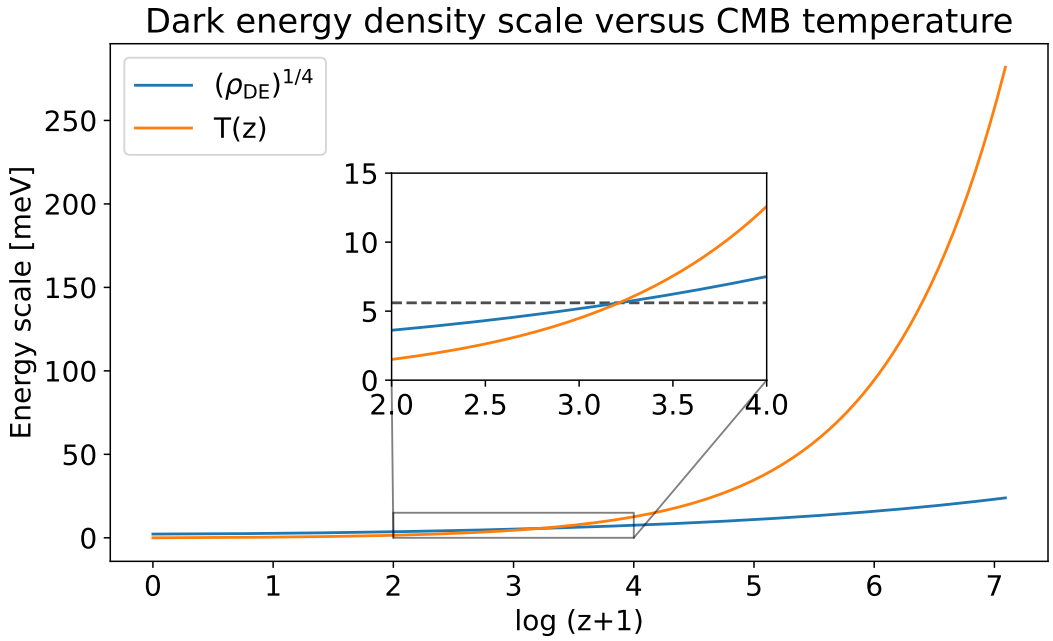

Figure 4.6: Dark energy scale $\rho_{\text{DE}}^{1/4}$ in units of meV. We compare this energy scale against the CMB temperature. As can be seen in this figure, the energy scale at which the CMB temperature and the dark-energy scale cross is equal to 5.6 meV when $z = 23.9$.

The most notable effect of matter creation as seen in fig. 4.5 is observed to happen when the dark-energy scale is comparable to the CMB temperature. We see in figure 4.6 that this happens around the multi-meV regime, which is the regime of the lightest neutrinos of the Standard Model. This hints that the particles created from our matter creation mechanism are light neutrinos. Note that these light neutrinos are mostly non-relativistic because the dark-energy scale corresponds with the rest mass energy of a light neutrino only. Consequently, these neutrinos are considered as matter instead of radiation. In particular, neutrinos are considered 'dark' due to their inability to interact with electromagnetic fields. This means they increase the dark matter component of the universe in our model.

The proportionality constant of our dynamic cosmological dark energy term C (see eqn. 2.37) might be indicative for the energy scale responsible for generating the dark-energy term. To extract this energy scale we take:

$$C^{1/3} = \left[\frac{9(H_0^{\text{late}})^2\Omega_{\beta,0}}{128(\pi G)^2}\right]^{1/6} = 23.76^{+0.36}_{-0.38}\ \text{MeV} \tag{4.3}$$

We predict that the creation of light neutrinos should be visible from late universe observations since the dark matter content should change as a function of redshift. Additionally, if we separate photons and neutrinos as two independent radiation components, the cosmic neutrino background could be significantly affected by this mechanism. The primordial neutrinos are mixed with the newly created neutrinos, which could seriously jeopardize the concept of a cosmic neutrino background to be studied.

It should be noted that these results are a 'first tentative calculation', as finding statistically correct values requires data and tools that are outside of the scope of this study. Similarly, our reverse engineering method to find $H_*^{\Lambda\text{-CDM}}$ from H_0^{early} (eqn. 3.1) might be an oversimplification. The reason for this is that the CMB analysis of the Planck collaboration assumes the Λ-CDM model and produces $H_0^{\Lambda\text{-CDM}}$ directly instead of using eqn. 3.1[4]. Their methodology

on how they produced $H_0^{\Lambda\text{-CDM}}$ is too elaborate for the scope of this study and requires more ongoing research.

4.2 The follow-up study: letting go of dark matter

Applying the fit procedure for this study, we find $z_* = 1105.8^{+0.91}_{-0.87}$ and $\Omega_{\beta,0} = 0.873^{+0.006}_{-0.006}$. Again applying eqn. 2.46 gives $\Omega_{M,0} = 0.102^{+0.005}_{-0.005}$. Similarly to the previous study of this chapter, we will present the results in the following figures.

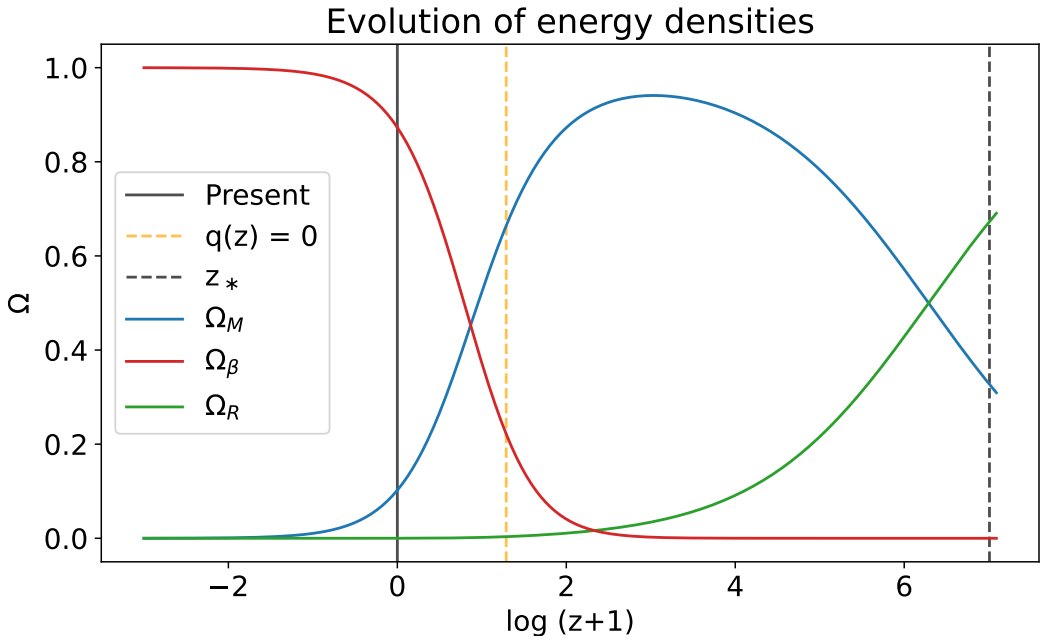

Figure 4.7: The evolved energy densities without dark matter.

If we compare figure 4.7 to figure 4.1, $\Omega_M(z_*)$ has to be much lower because we don't include dark matter anymore in our model. Consequently, $\Omega_{\beta,0}$ has to be much higher, resulting in a shorter epoch of matter dominance and substantially later moment of matter-radiation equality at $z = 537.1$. Additionally, $\Omega_{M,0}$ has been reduced by a factor of 4.3 because of the increase in $\Omega_{\beta,0}$. This means our model predicts a significant reduction in the contribution of matter density to the universe in the early universe as well as in the present, late universe.

4.2.1 Accelerated expansion in the follow-up study

Following the same procedure as in the previous study, we will decide from figure 4.8 our region of validation.

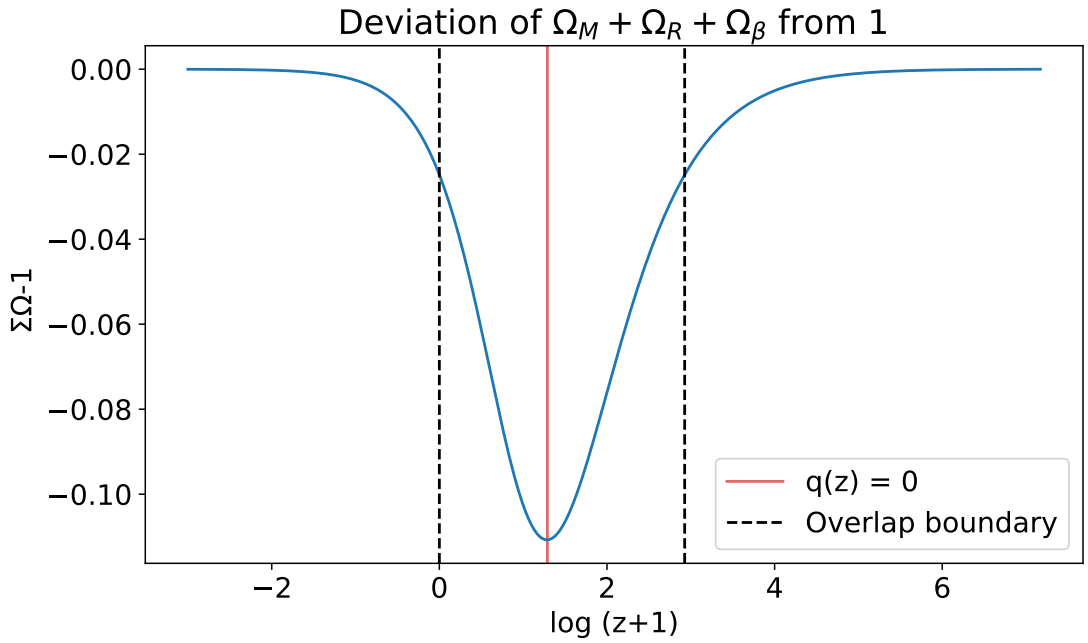

Figure 4.8: Deviation from the Λ-CDM model as explained in fig 4.2. This time, we observe a much larger region of validation of $z \in [0, 17.67]$. Again, the validation region will be the x-axis range for figure 4.9.

As explained in section 4.1.1, figure 4.8 describes how our dynamical dark energy density differs from a constant dark energy density. It shows that the present day ($z = 0$) universe has almost reached the constant dark energy density regime. Additionally, we see in figure 4.8 that the graph has shifted to the right compared to 4.2. This means that our model is now very similar to the Λ-CDM model at present time compared to figure 4.2. This leads to a larger deviation from Λ-CDM in the late universe compared to figure 4.2. This means the Hubble parameter decreases substantially less from z_* to $z = 0$ to fit the Hubble tension in the follow-up study compared to the main study.

This is expected because the dark matter contribution is removed from eqn. 3.28. Consequently, $H_* < H_*^{\Lambda\text{-CDM}}$ (see eqns. 3.28 and 3.1 respectively), which means that the increase of the Hubble parameter over the course of its evolution backward in time has decreased to reach a lower value in the early universe.

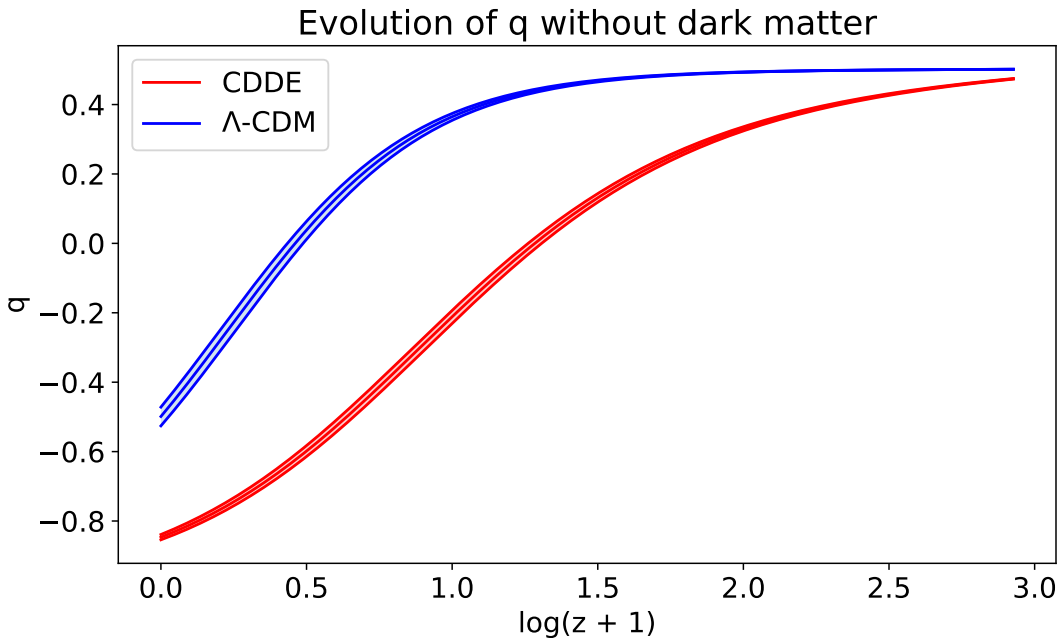

Figure 4.9: Deceleration parameter in the validation region according to figure 4.8. This graph shows no overlap unfortunately, which means that low redshift measurements are not compatible with our CDDE model without dark matter. This is expected, because increasing the amount of dark energy in the universe results in a larger acceleration of the universe. The difference between our model and the Λ-CDM model decreases as we go to higher redshifts, but the ideal scenario is an overlap at $z \leq 1$ as this is the common redshift range for late universe observations [1, 15].

As can be seen from figure 4.9, there is no overlap between our CDDE model without dark matter and the Λ-CDM model. In fact, it deviates to such an extent that we can refer to it as an 'acceleration tension'. This is a result from the increased dark energy content, which increases the acceleration of the scale factor ($\ddot{a}$). This acceleration is necessary to link H_0^{late} to the lower value of H_* in the early universe. We conclude from figure 4.9 that dark matter is not only required to describe the Hubble parameter in the early universe (as will be shown in section 4.2.2) but also required to explain the acceleration in the late universe.

4.2.2 Matter creation in the follow-up study

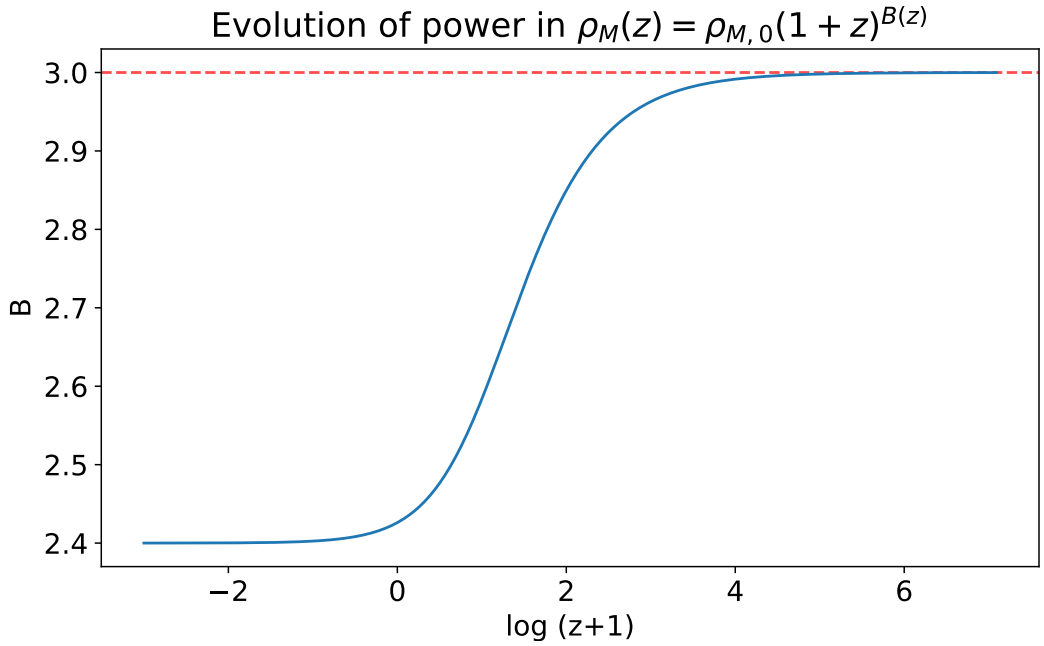

Figure 4.10: Power law of $\rho_M(z)$ in the follow-up study. In this study, matter creation happens earlier at $z \approx 22$, compared to $z \approx 9$ for the first model that includes dark matter. This means there has been more time for matter creation.

Given the new fit values given in section 4.2 our follow-up study predicts $f_M = 2.45$. This is unfortunately not enough to produce all required dark matter, as this should be closer to a factor of 5 or 6 [1]. Additionally, this model does not predict the same late universe observations as Λ-CDM (see figure 4.9). This is due to the dark energy contribution which causes the universe to accelerate faster than is observed.

Similarly to the previous study, these results should be taken as a first approximation. However, even as a first approximation, it is clear that the matter creation mechanism in our dynamical dark energy model is not able to fully account for all observed dark matter. To check if this model has any capability to provide a sufficient level of mass creation, we perform a parameter sweep over $\Omega_{\beta,0}$ and record f_M with its respective q_0. This is shown in figure 4.11.

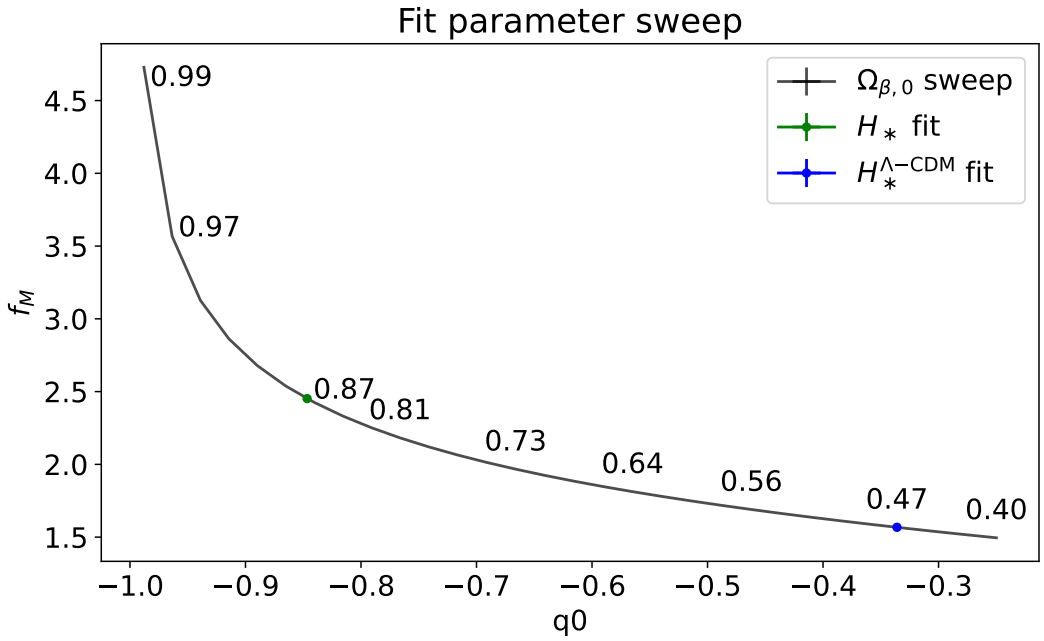

Figure 4.11: Fit parameter sweep with its corresponding mass creation factor f_M and deceleration parameter q_0. The black line represents increasing values of $\Omega_{\beta,0}$. The line starts on the right with $\Omega_{\beta,0} = 0.4$ and ends on the left with $\Omega_{\beta,0} = 0.99$. This plot does contain errorbars, however these are too small to see.

From figure 4.11 we see that f_M increases steeply for values of $\Omega_{\beta,0}$ very close to 1, but as a consequence the universe is predicted to accelerate in an unacceptable fashion.

5 CONCLUSIONS AND OUTLOOK

In this study we proposed an alternative model to Λ-CDM by introducing a matter creation mechanism through a curvature dependent dark energy (CDDE) term with the purpose to solve the Hubble tension. This was achieved by numerically evolving the Hubble parameter using the dark energy content in the present universe $\Omega_{\beta,0}$ as a fit parameter. By applying the fitting method, we successfully solved the Hubble tension with $\Omega_{\beta,0} = 0.465^{+0.033}_{-0.034}$. The viability of this solution has been verified by calculating the deceleration parameter $q(z)$ using our model and comparing it with the Λ-CDM predicted version. Although our model was only constructed to solve the Hubble tension, it was also found to be compatible with the measured acceleration of the expansion of the universe. Our model predicts an increase of the total matter content in the universe by 57%. This consists of light non-relativistic neutrinos with a rest mass energy of multiple meV. These neutrinos are counted towards the dark matter contribution in the universe because of their inability to interact with electromagnetic fields.

Our model predicts an observable change in the matter content in the universe for redshifts $z \leq 9$. This is an integrated effect that could potentially be visbile in the cosmic neutrino background as the introduction of newly created neutrinos could have a blurring effect. Additionally, we predict the dark matter content could decrease at higher redshifts, which could be an observable effect. Another integrated effect from our model stems from the dynamical dark energy density. Its differential contribution to the Hubble parameter in the CDDE model is negligible in the early universe, but when integrated over a large redshift interval, it introduces a small yet observable deviation from the standard Λ-CDM based Hubble parameter. This could be an even larger observable effect when integrated over even larger redshift intervals, and should thus be accounted for when using the Hubble parameter in the CDDE model beyond the late universe.

Integrated dark energy effects and matter creations effects could have an effect on early universe measurements of time and distance intervals since they are derived from integrating over the Hubble parameter from present day to the early universe. One of such distance measurements is the location of the first peak of the power spectrum of the CMB density fluctuations which is used to derive the sound horizon of acoustic oscillations in the primordial plasma. Another effect that feels the influence from dark energy is the integrated Sachs-Wolfe effect and should be accounted for if the integrated Sachs-Wolfe effect is studied in more detail using this model. The results of this study are a 'first tentative calculation' and do not yield any statistical value. This requires access to tools and datasets that are outside the scope of this study and could be the subject of a follow-up study.

As a follow-up study, we took our matter creation mechanism to the extreme and tested if it could create enough dark matter to serve as an explanation for dark matter. This was done by assuming that the Hubble parameter in the early universe is described by a two component universe consisting of baryonic matter and radiation exclusively. By fitting our model such that our Hubble parameter matches this new assumed Hubble parameter in the early universe, we find $\Omega_{\beta,0} = 0.873^{+0.006}_{-0.006}$. From the follow-up study we find the total matter content to be enhanced by

a factor of 2.45. This is unfortunately not enough to provide a consistent explanation for all the dark matter content in the universe, as the matter creation factor would in that case be required to be between 5 and 6 [1]. In addition, by increasing the dark energy content to increase the matter content over-accelerates the universe, making it incompatible with late universe observations.

References

[1] Barbara Ryden. “Introduction to Cosmology”. In: *Introduction to cosmology / Barbara Ryden. San Francisco, CA, USA: Addison Wesley, ISBN 0-8053-8912-1, 2003, IX + 244 pp.* (Oct. 2003). doi: 10.1063/1.1825274.

[2] Licia Verde, Tommaso Treu, and Adam G Riess. “Tensions between the early and late Universe”. In: *Nature Astronomy* 3 (Sept. 2019), pp. 891–895. doi: 10.1038/s41550-019-0902-0.

[3] Adam G. Riess et al. “A Comprehensive Measurement of the Local Value of the Hubble Constant with 1 km s−1 Mpc−1 Uncertainty from the Hubble Space Telescope and the SH0ES Team”. In: *The Astrophysical Journal Letters* 934 (July 2022), p. L7. issn: 2041-8205. doi: 10.3847/2041-8213/AC5C5B. url: https://iopscience.iop.org/article/10.3847/2041-8213/ac5c5b%20https://iopscience.iop.org/article/10.3847/2041-8213/ac5c5b/meta.

[4] N. Aghanim et al. “Planck 2018 results - VI. Cosmological parameters”. In: *Astronomy & Astrophysics* 641 (Sept. 2020), A6. issn: 0004-6361. doi: 10.1051/0004-6361/201833910. url: https://www.aanda.org/articles/aa/full_html/2020/09/aa33910-18/aa33910-18.html%20https://www.aanda.org/articles/aa/abs/2020/09/aa33910-18/aa33910-18.html.

[5] Wim Beenakker and David Venhoek. “A structured analysis of Hubble tension”. In: (Jan. 2021). url: https://arxiv.org/abs/2101.01372v2.

[6] Richard H. Cyburt, Brian D. Fields, and Keith A. Olive. “Primordial nucleosynthesis in light of WMAP”. In: *Physics Letters* B567 (Aug. 2003), pp. 227–234. issn: 0370-2693. doi: 10.1016/J.PHYSLETB.2003.06.026.

[7] *File:The History of the Universe.jpg - Wikimedia Commons*. url: https://commons.wikimedia.org/wiki/File:The_History_of_the_Universe.jpg.

[8] P J E Peebles. “Recombination of the Primeval Plasma”. In: *Astrophys. J.* 153 (1968), p. 1. doi: 10.1086/149628.

[9] *Rodney Loudon-The Quantum Theory of Light, 3rd Ed. (Oxford Science Publications) - Oxford University Press, USA (2000) | PDF*. url: https://www.scribd.com/document/341409947/Rodney-Loudon-The-Quantum-Theory-of-Light-3rd-Ed-Oxford-Science-Publications-Oxford-University-Press-USA-2000.

[10] T Padmanabhan. *Structure Formation in the Universe*. Cambridge UK: Cambridge University Press, June 1993. isbn: 9780521424868.

[11] *CMB: Sound Waves in the Early Universe*. url: https://astro.uchicago.edu/~frieman/Courses/A411-old/Lecture8/Lecture8-2010.pdf.

[12] Bruce Bassett and Renée Hlozek. “Baryon acoustic oscillations”. In: *Dark Energy: Observational and Theoretical Approaches*. Ed. by Pilar Ruiz-Lapuente. Cambridge: Cambridge University Press, 2010, pp. 246–278. isbn: 9780521518888. doi: DOI:10.1017/CBO9781139193627.010.

[13] Leandro Manuel Pardo Calderón. “Baryon Acoustic Oscillations. Equation and physical interpretation”. In: *Scientia Et Technica* 23 (June 2018), pp. 262–267. url: https://www.redalyc.org/journal/849/84958001016/html/.

[14] *Galaxies and the Universe - Large-Scale Structure*. url: https://pages.astronomy.ua.edu/keel/galaxies/largescale.html.

[15] T Padmanabhan. “Cosmological constant—the weight of the vacuum”. In: *Physics Reports* 380 (2003), pp. 235–320. issn: 0370-1573. doi: https://doi.org/10.1016/S0370-1573(03)00120-0. url: https://www.sciencedirect.com/science/article/pii/S0370157303001200.

[16] D. J. Fixsen. “THE TEMPERATURE OF THE COSMIC MICROWAVE BACKGROUND”. In: *The Astrophysical Journal* 707 (Nov. 2009), p. 916. issn: 0004-637X. doi: 10.1088/0004-637X/707/2/916. url: https://iopscience.iop.org/article/10.1088/0004-637X/707/2/916.

[17] *Energy in Radiation in the Early Universe*. url: http://hyperphysics.phy-astr.gsu.edu/hbase/Astro/engrad.html#c3.

[18] Dillon Brout et al. “The Pantheon+ Analysis: Cosmological Constraints”. In: *The Astrophysical Journal* 938 (Oct. 2022), p. 110. issn: 0004-637X. doi: 10.3847/1538-4357/AC8E04. url: https://iopscience.iop.org/article/10.3847/1538-4357/ac8e04%20https://iopscience.iop.org/article/10.3847/1538-4357/ac8e04/meta.

[19] Manuel Peimbert. “The primordial helium abundance”. In: *Current Science* 95 (2008), pp. 1165–1176. issn: 00113891. url: http://www.jstor.org/stable/24103231.

[20] Manuel Peimbert, Valentina Luridiana, and Antonio Peimbert. “Revised Primordial Helium Abundance Based on New Atomic Data”. In: *The Astrophysical Journal* 666 (Sept. 2007), pp. 636–646. issn: 0004-637X. doi: 10.1086/520571/FULLTEXT/. url: https://iopscience.iop.org/article/10.1086/520571%20https://iopscience.iop.org/article/10.1086/520571/meta.

[21] *IONIZATION, SAHA EQUATION*. url: https://www.astro.princeton.edu/~gk/A403/ioniz.pdf.

[22] *Propagation of Error*. url: https://academics.hamilton.edu/physics/smajor/courses/195Guides/phys190_uncertainties_II.pdf.